Modeling the Heliosphere: Status and future directions

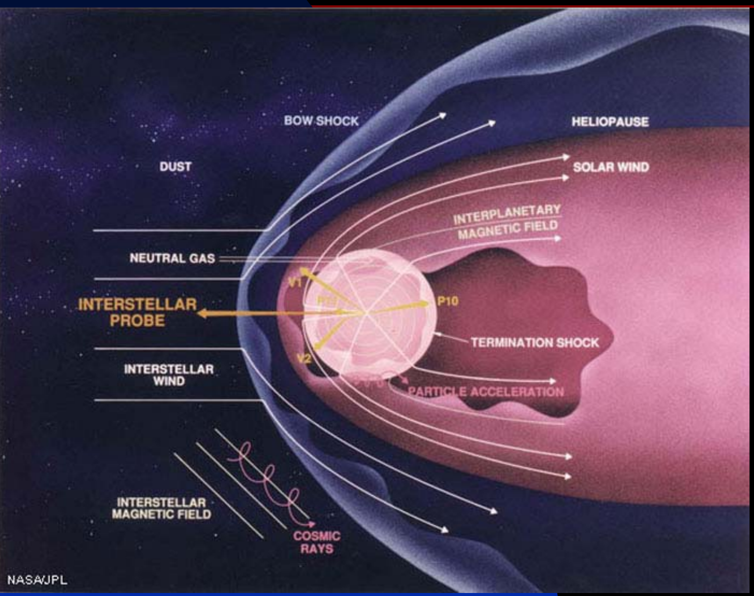

G.P. Zank, N. Pogorelov, V. Florinski,
J. Heerikhuisen, H.-R. Mueller

Institute of Geophysics and Planetary Physics (IGPP)
University of California, Riverside

Supported in part by an NSF ITR grant and several NASA grants

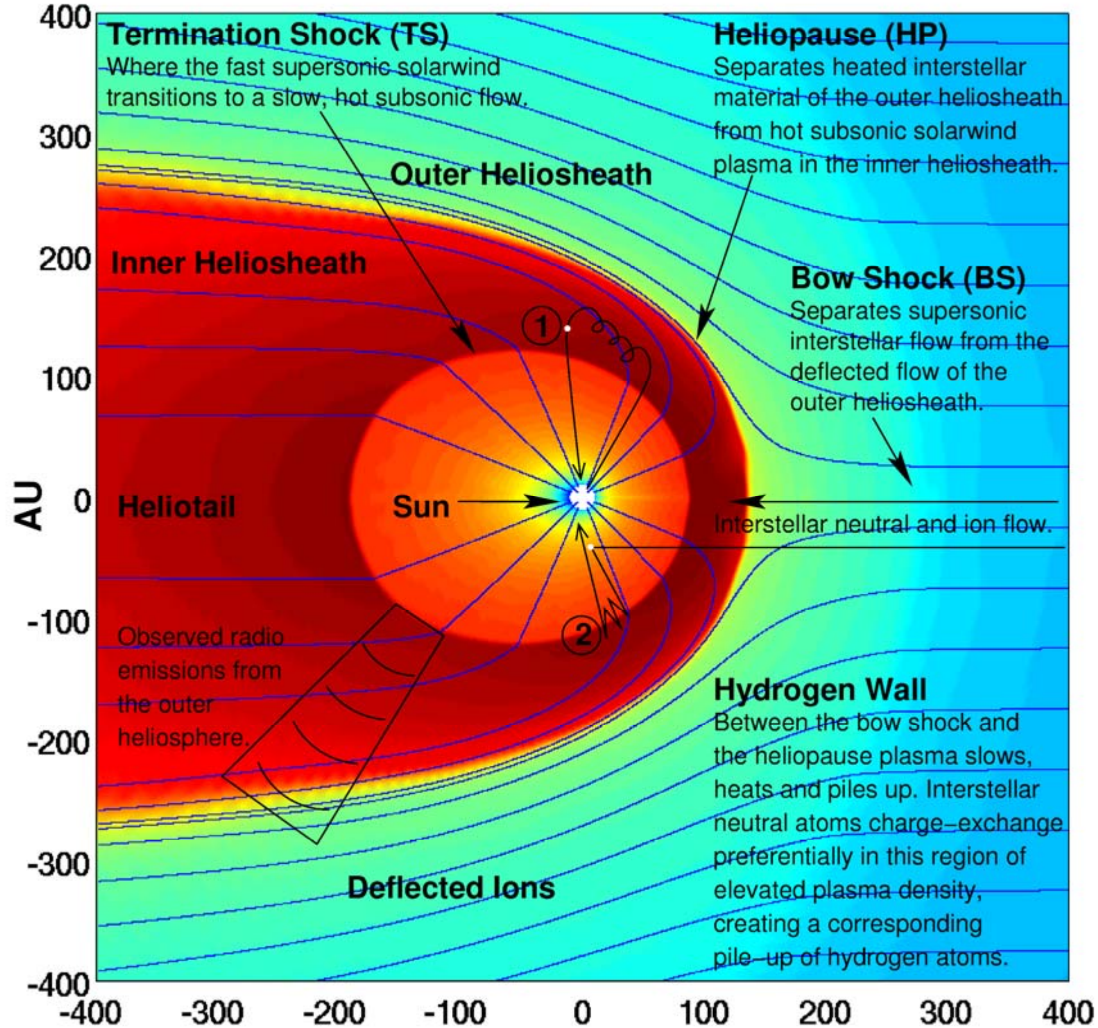

1 A solar wind proton travels into the hot inner heliosheath where it charge–exchanges with an interstellar hydrogen atom to create an energetic neutral atom (ENA).

2 An interstellar neutral atom charge–exchanges in the supersonic solar wind to form a a pick–up ion (PUI), which is energized at the termination shock to produce an anomalous cosmic ray (ACR).

Color contours of plasma temperature with streamlines from a self–consistent Monte–Carlo simulation by J. Heerikhuisen, V. Florinski and G. P. Zank.

Three Distinct Neutral Populations

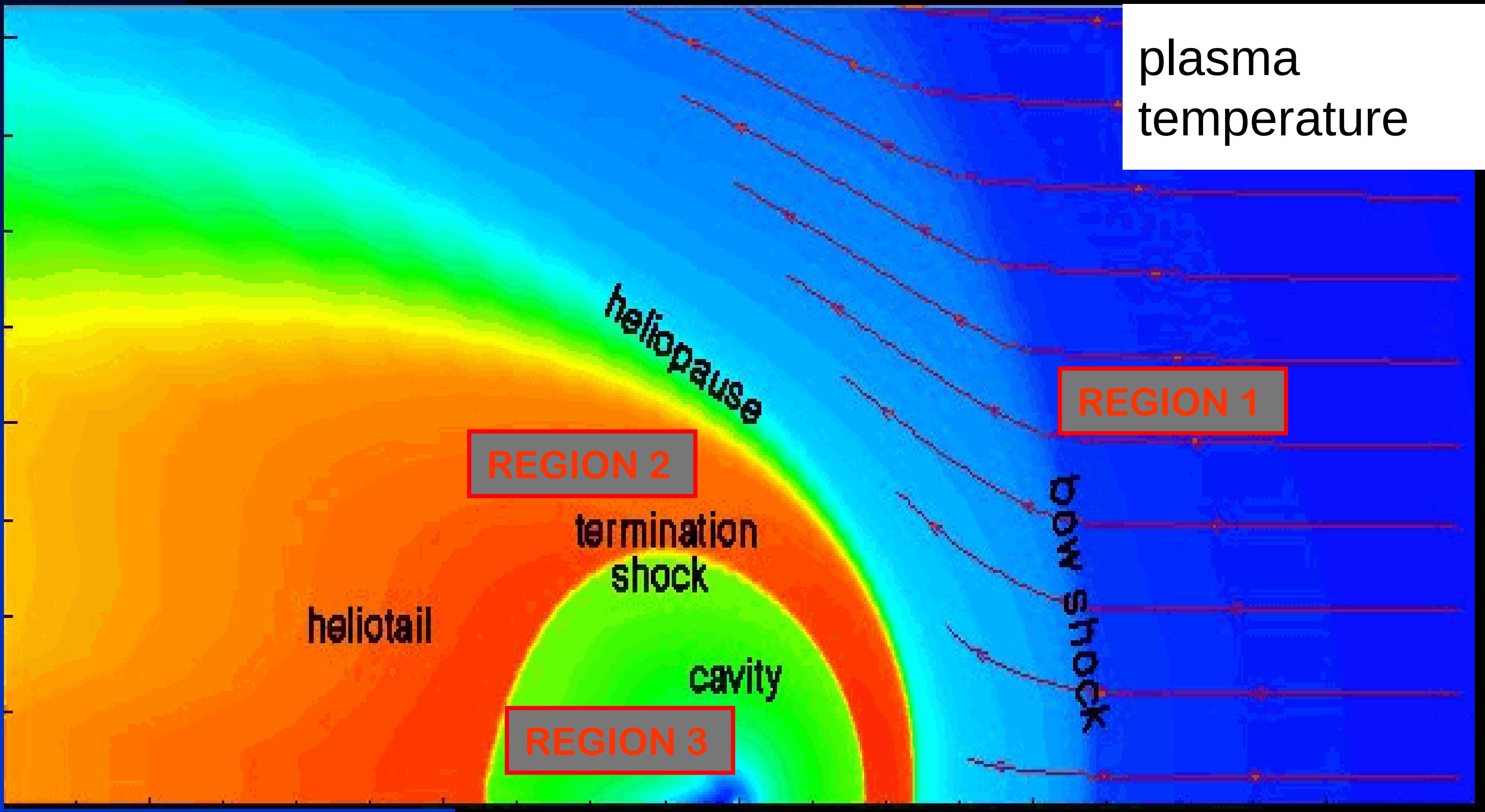

The Outer Heliosphere and the LISM

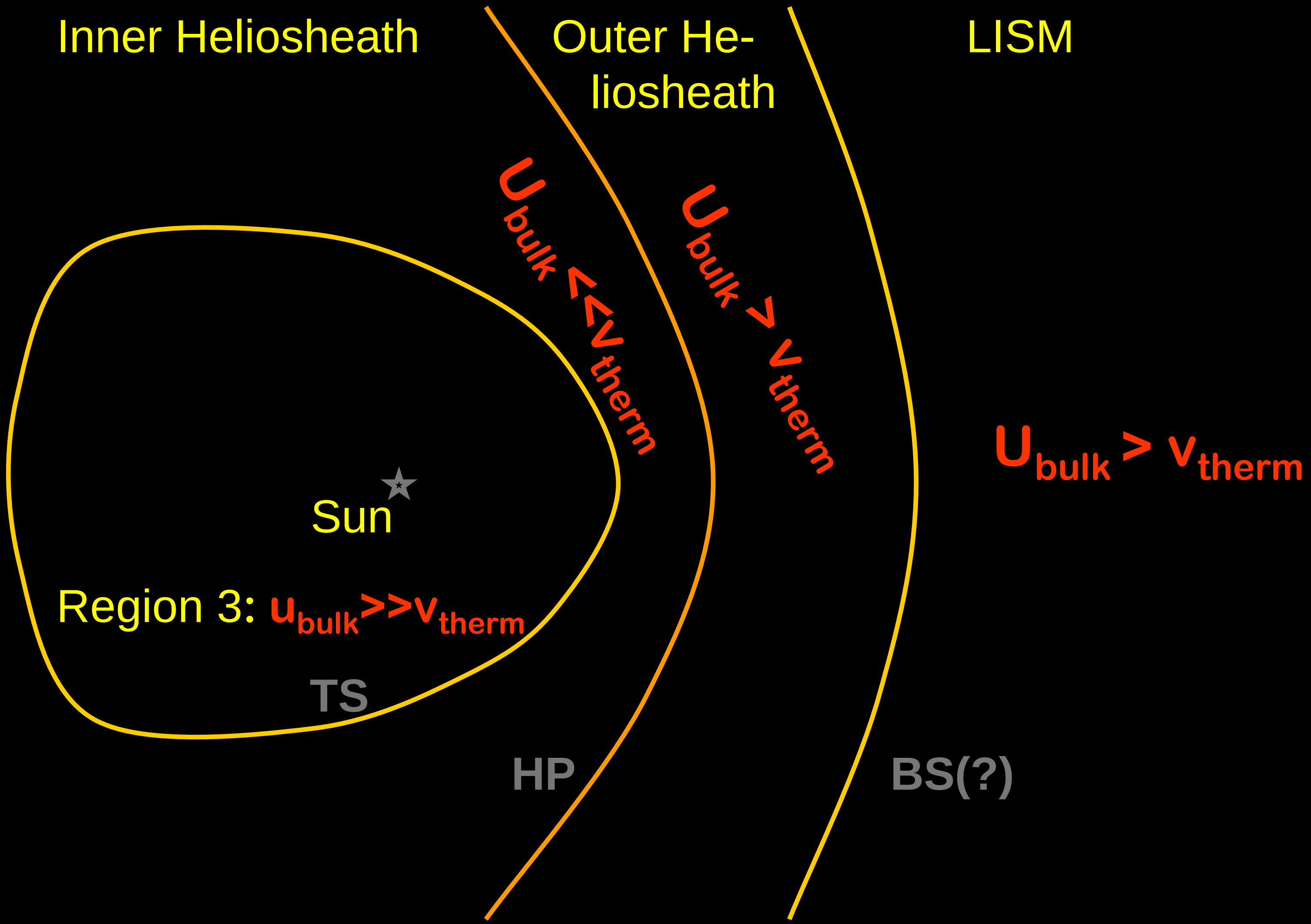

Charge Exchange Interaction

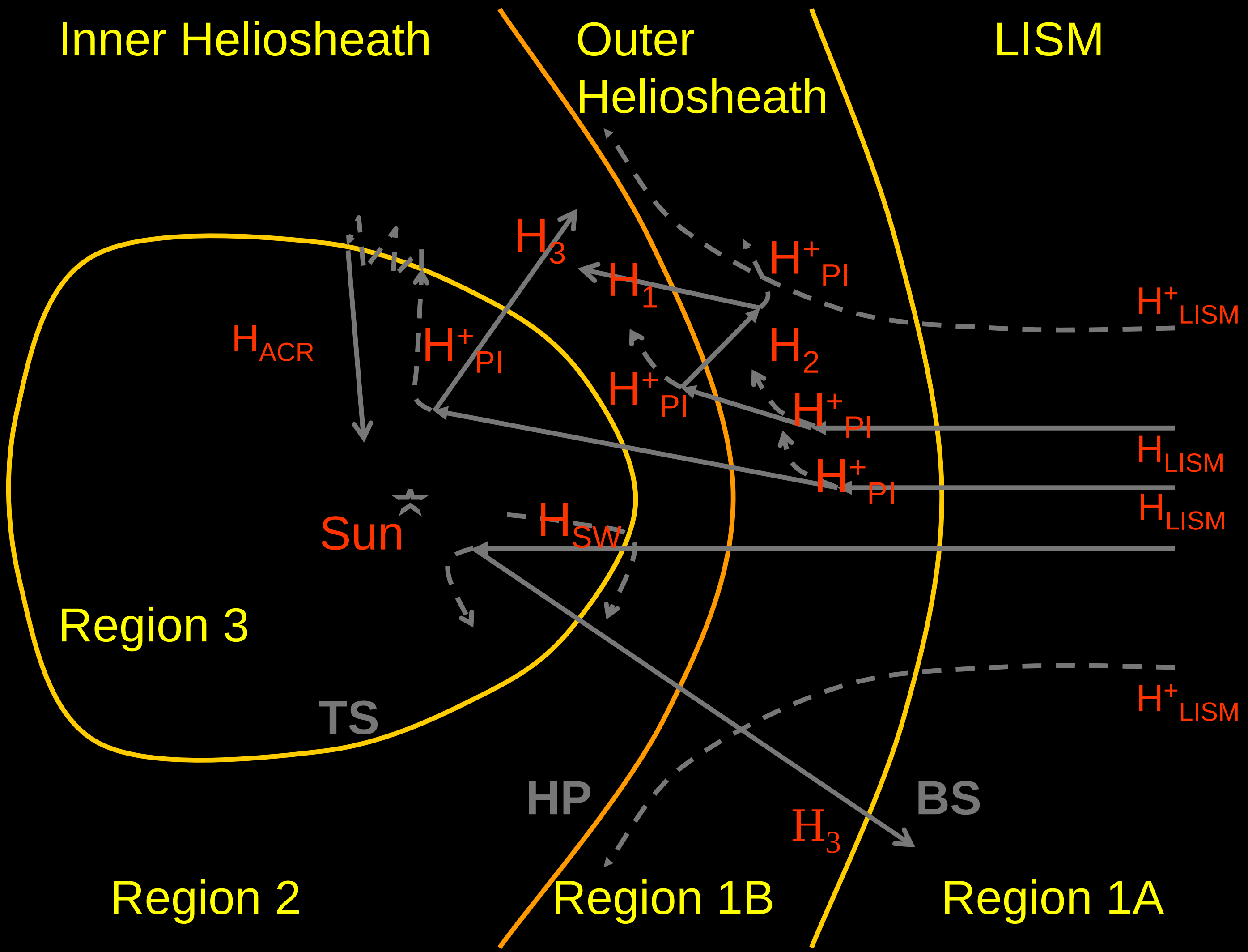

Plasma Interactions: plasma-neutral

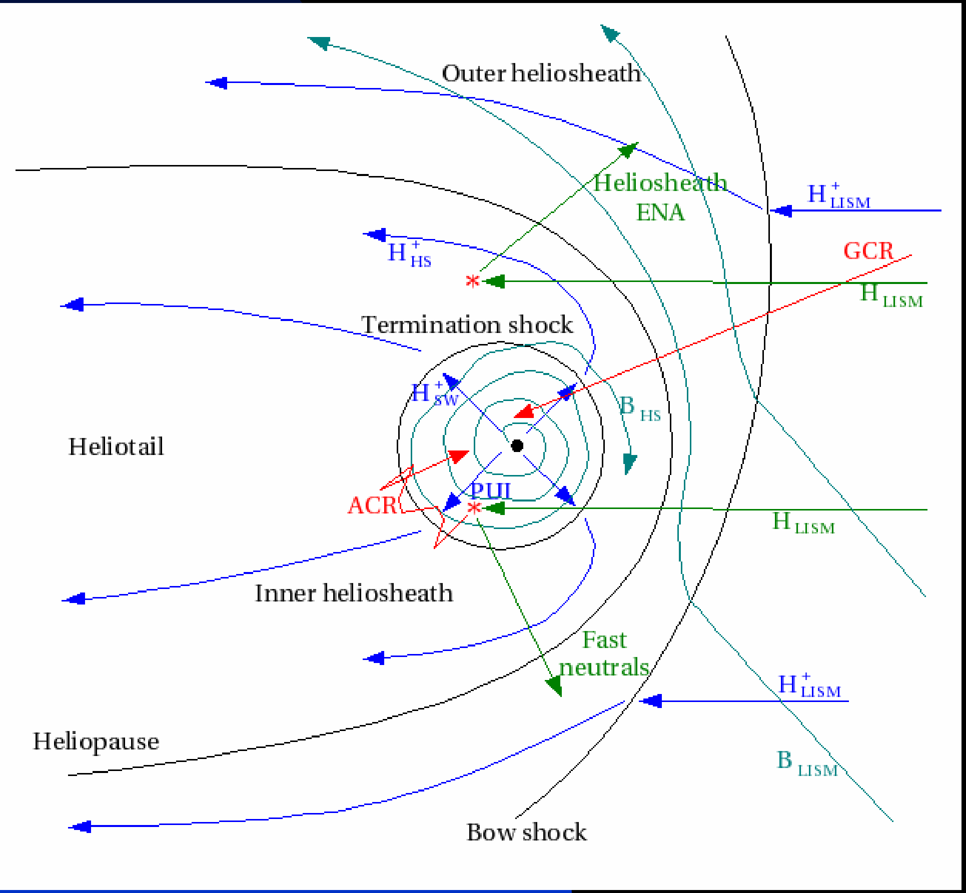

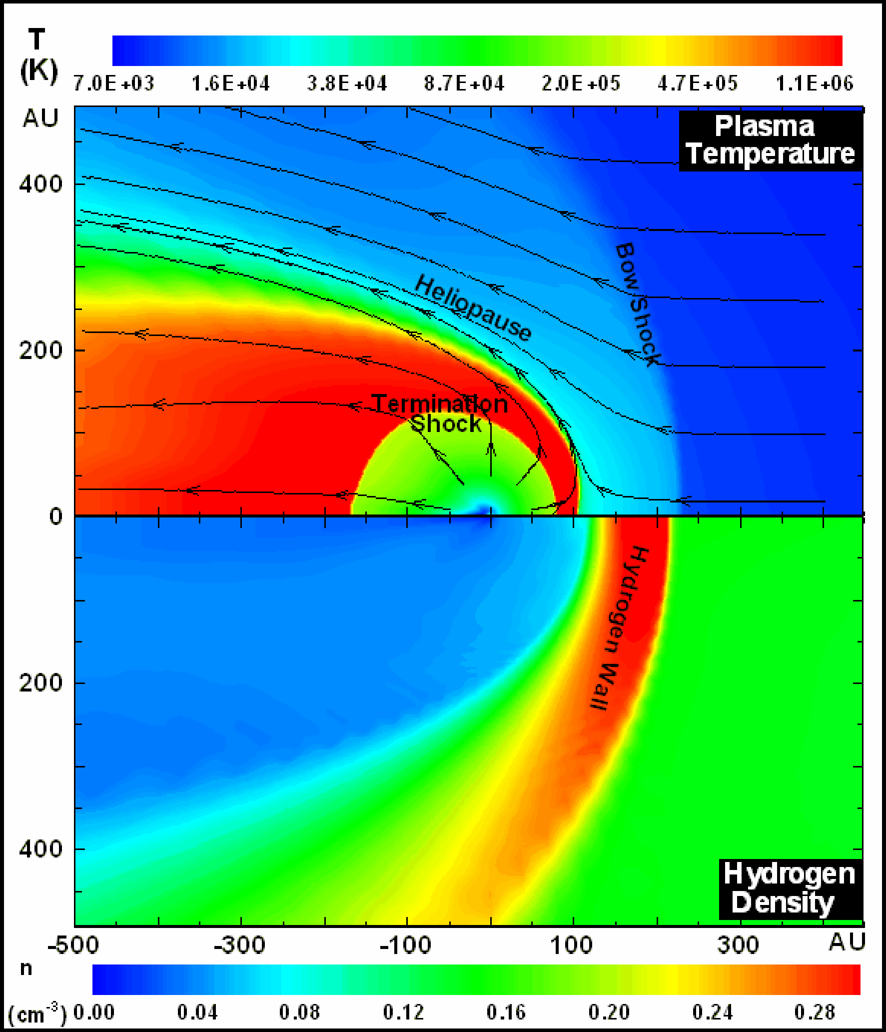

Numerical Models of the Heliosphere: Atoms and Hydrodynamics

- Self-consistent models:
  - dynamic plasma and neutrals: four-fluid model,
  - Monte-Carlo Boltzmann, particle Boltzmann.

Four-Fluid Concept

Fluid 0: plasma

Origin: Sun and LISM, and all charge exchange (pickup ions)

Neutral Fluid 2

Origin: Charge exchange between termination shock and heliopause

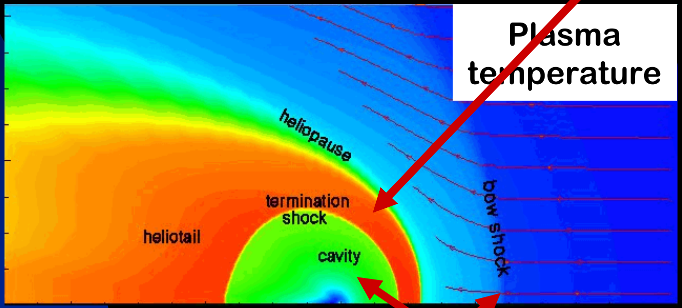

≈ 100km/s, “random” direction; hot

Neutral Fluid 1

Origin: LISM, and charge exchange outside heliopause

Neutral Fluid 3

Origin: Charge exchange with solar wind (inside termination shock)

≈20km/s, LISM direction

warm

400km/s, radial direction

cold

Four-fluid model

Fluid 0: plasma

Origin: Sun and LISM, and all charge exchange (pickup ions)

$$\begin{aligned} \frac{\partial \rho}{\partial t} + \nabla \cdot (\rho \mathbf{u}) &= 0, \\ \frac{\partial}{\partial t}(\rho \mathbf{u}) + \nabla \cdot (\rho \mathbf{u}\mathbf{u}) + \nabla p &= \mathbf{Q_m}, \\ \frac{\partial}{\partial t}\left(\frac{1}{2}\rho u^2 + \frac{p}{\gamma - 1}\right) + \nabla \cdot \left(\frac{1}{2}\rho u^2 \mathbf{u} + \frac{\gamma}{\gamma - 1} p\mathbf{u}\right) &= Q_e, \end{aligned}$$

Neutral Fluid 2

Origin: Charge exchange between termination shock and heliopause

$$\begin{aligned} \frac{\partial \rho}{\partial t} + \nabla \cdot (\rho \mathbf{u}) &= 0, \\ \frac{\partial}{\partial t}(\rho \mathbf{u}) + \nabla \cdot (\rho \mathbf{u}\mathbf{u}) + \nabla p &= \mathbf{Q_m}, \\ \frac{\partial}{\partial t}\left(\frac{1}{2}\rho u^2 + \frac{p}{\gamma - 1}\right) + \nabla \cdot \left(\frac{1}{2}\rho u^2 \mathbf{u} + \frac{\gamma}{\gamma - 1} p\mathbf{u}\right) &= Q_e, \end{aligned}$$

0
1
3

Neutral Fluid 1

Origin: LISM, and charge exchange outside heliopause

$$\begin{aligned} \frac{\partial \rho}{\partial t} + \nabla \cdot (\rho \mathbf{u}) &= 0, \\ \frac{\partial}{\partial t}(\rho \mathbf{u}) + \nabla \cdot (\rho \mathbf{u}\mathbf{u}) + \nabla p &= \mathbf{Q_m}, \\ \frac{\partial}{\partial t}\left(\frac{1}{2}\rho u^2 + \frac{p}{\gamma - 1}\right) + \nabla \cdot \left(\frac{1}{2}\rho u^2 \mathbf{u} + \frac{\gamma}{\gamma - 1} p\mathbf{u}\right) &= Q_e, \end{aligned}$$

0
2
3

Neutral Fluid 3

Origin: Charge exchange with solar wind (inside termination shock)

$$\begin{aligned} \frac{\partial \rho}{\partial t} + \nabla \cdot (\rho \mathbf{u}) &= 0, \\ \frac{\partial}{\partial t}(\rho \mathbf{u}) + \nabla \cdot (\rho \mathbf{u}\mathbf{u}) + \nabla p &= \mathbf{Q_m}, \\ \frac{\partial}{\partial t}\left(\frac{1}{2}\rho u^2 + \frac{p}{\gamma - 1}\right) + \nabla \cdot \left(\frac{1}{2}\rho u^2 \mathbf{u} + \frac{\gamma}{\gamma - 1} p\mathbf{u}\right) &= Q_e, \end{aligned}$$

0
1
2

Hybrid Boltzmann model

Kinetic description: neutral distribution function

Origin: LISM, and all charge exchange

$$\frac{\partial}{\partial t} f_H + \mathbf{v}\cdot\nabla f_H + \frac{\mathbf{F}}{m_p}\cdot\nabla_{\mathbf{v}} f_H = P - L$$

production

loss

Fluid: plasma

Origin: Sun and LISM, and all charge exchange (pickup ions)

$$\begin{aligned}
\frac{\partial \rho}{\partial t} + \nabla\cdot(\rho\mathbf{u}) &= 0, \\
\frac{\partial}{\partial t}(\rho\mathbf{u}) + \nabla\cdot(\rho\mathbf{u}\mathbf{u}) + \nabla p &= \mathbf{Q}_m, \\
\frac{\partial}{\partial t}\left(\frac{1}{2}\rho u^2 + \frac{p}{\gamma-1}\right) + \nabla\cdot\left(\frac{1}{2}\rho u^2\mathbf{u} + \frac{\gamma}{\gamma-1}p\mathbf{u}\right) &= Q_e,
\end{aligned}$$

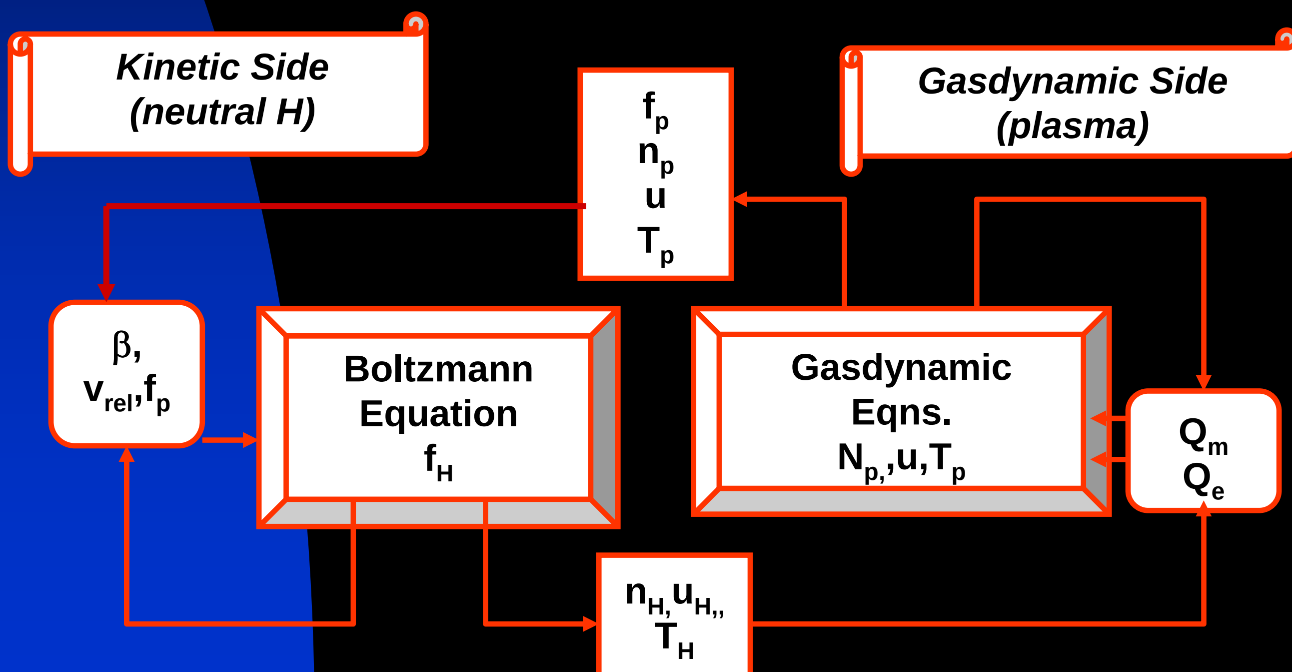

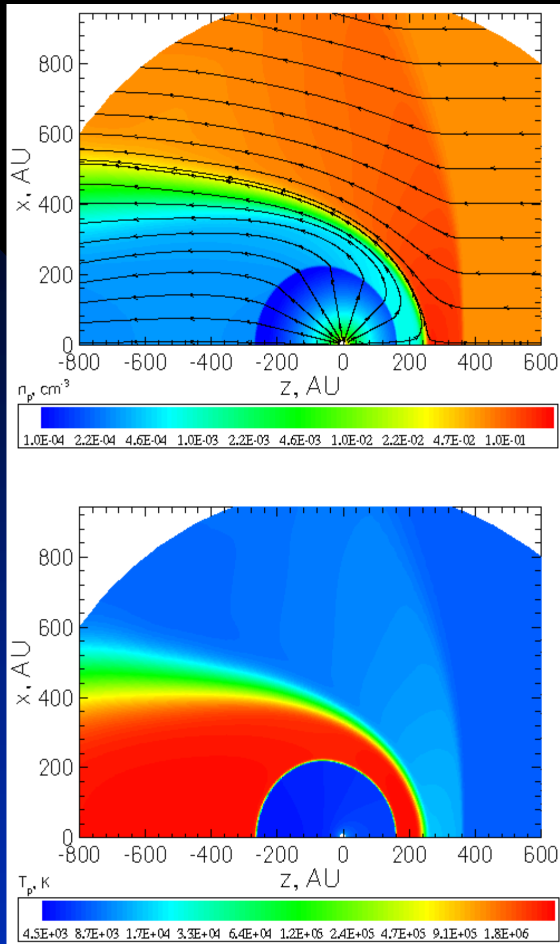

without H atoms

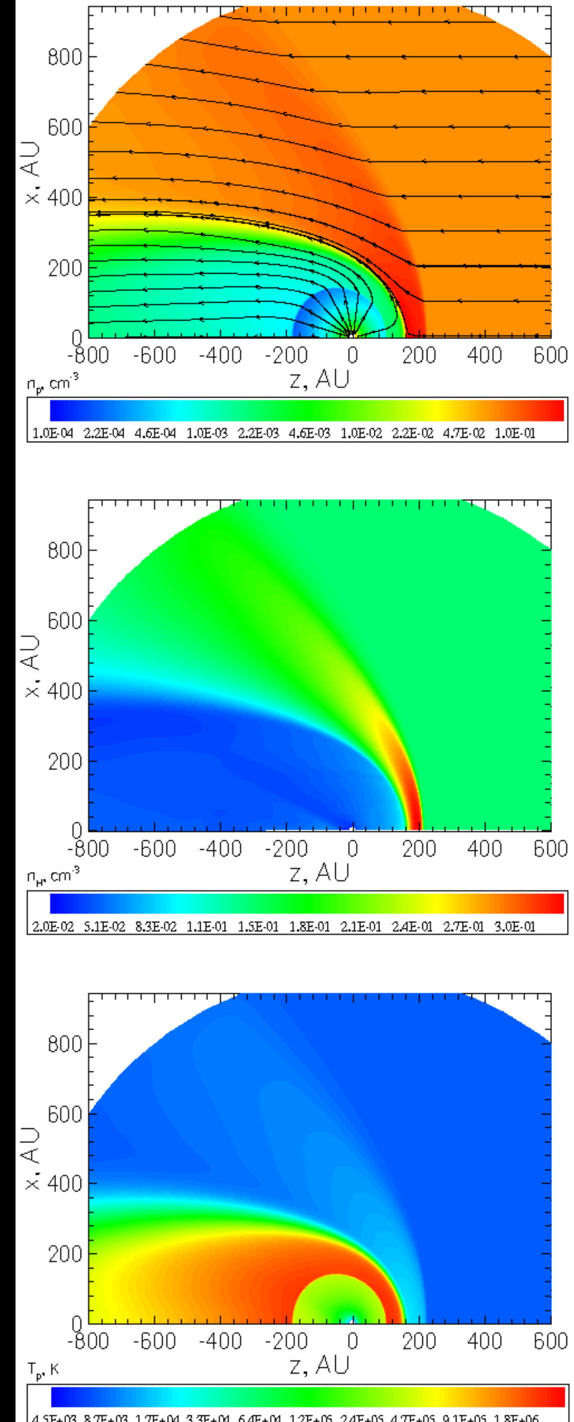

with H atoms

Heliospheric Structure

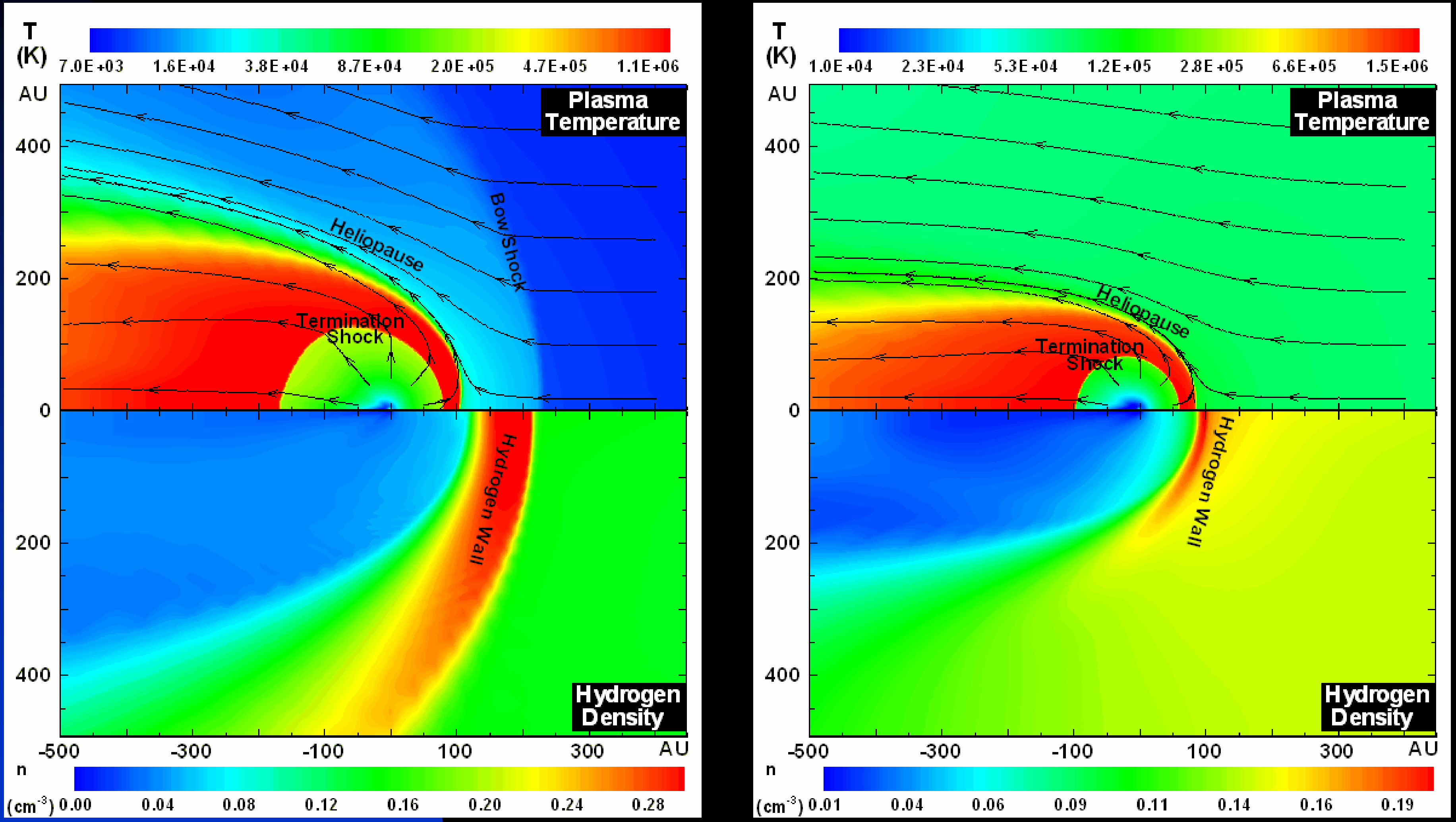

2-shock model

1-shock model

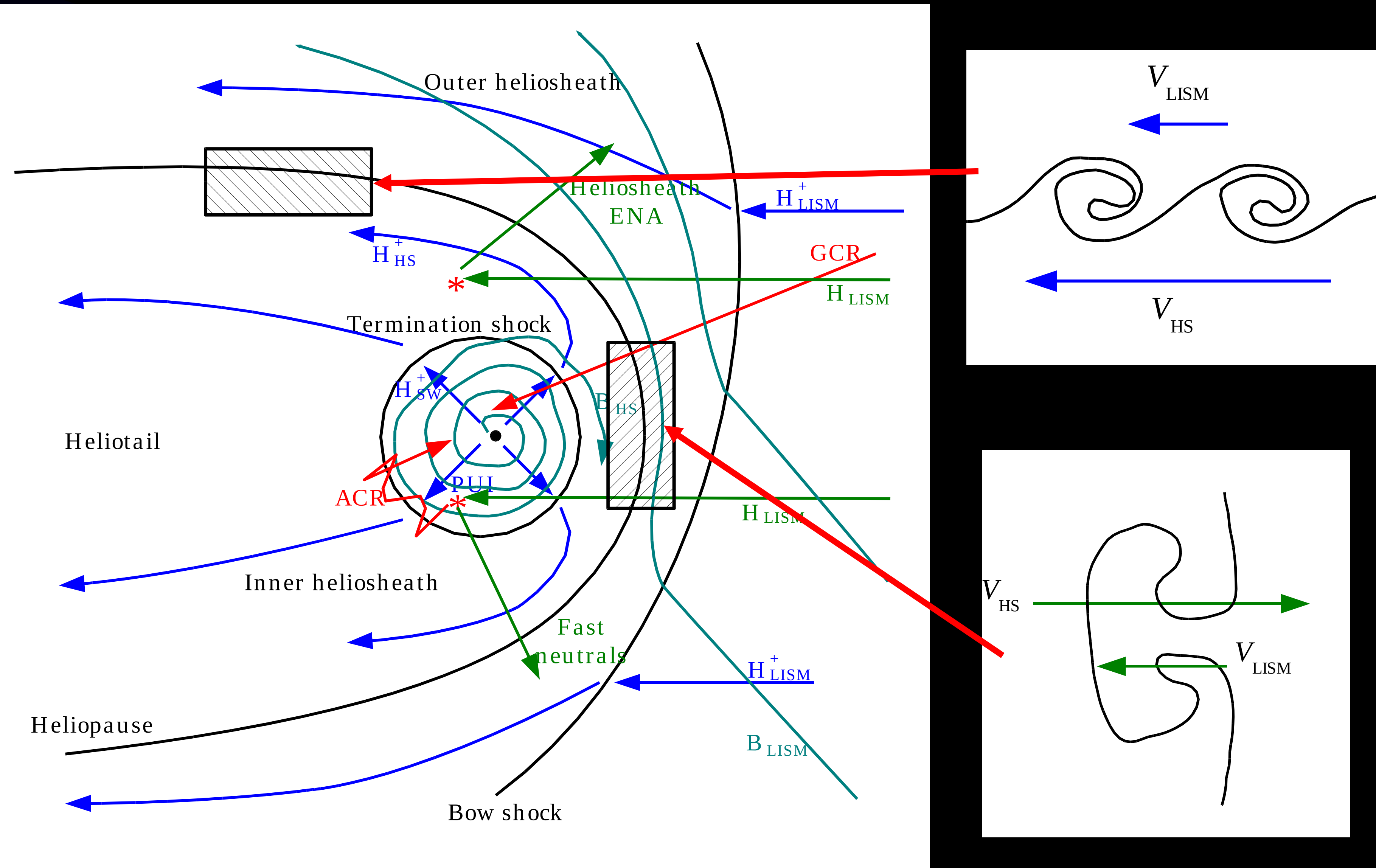
Outer heliosheath
Heliosheath
ENA
H^+_{LISM}
GCR
H^+_{HS}
H_{LISM}
Termination shock
H^+_{SW}
B_{HS}
Heliotail
PUI
ACR
H_{LISM}
Inner heliosheath
Fast
neutrals
H^+_{LISM}
Heliopause
B_{LISM}
Bow shock
V_{LISM}
V_{HS}
V_{HS}
V_{LISM}

Simulations

1. Quasi-equilibrium state
2. Instability triggered by perturbations from previous cycle
3. Instability develops. Mushroom-shape structures are a signature of R-T
4, 5: Structure is advected along the heliopause. Relaxation phase.
6. Return to the quasi-equilibrium

1 cycle = 100 years

TS oscillates with an amplitude of ~ 3 AU

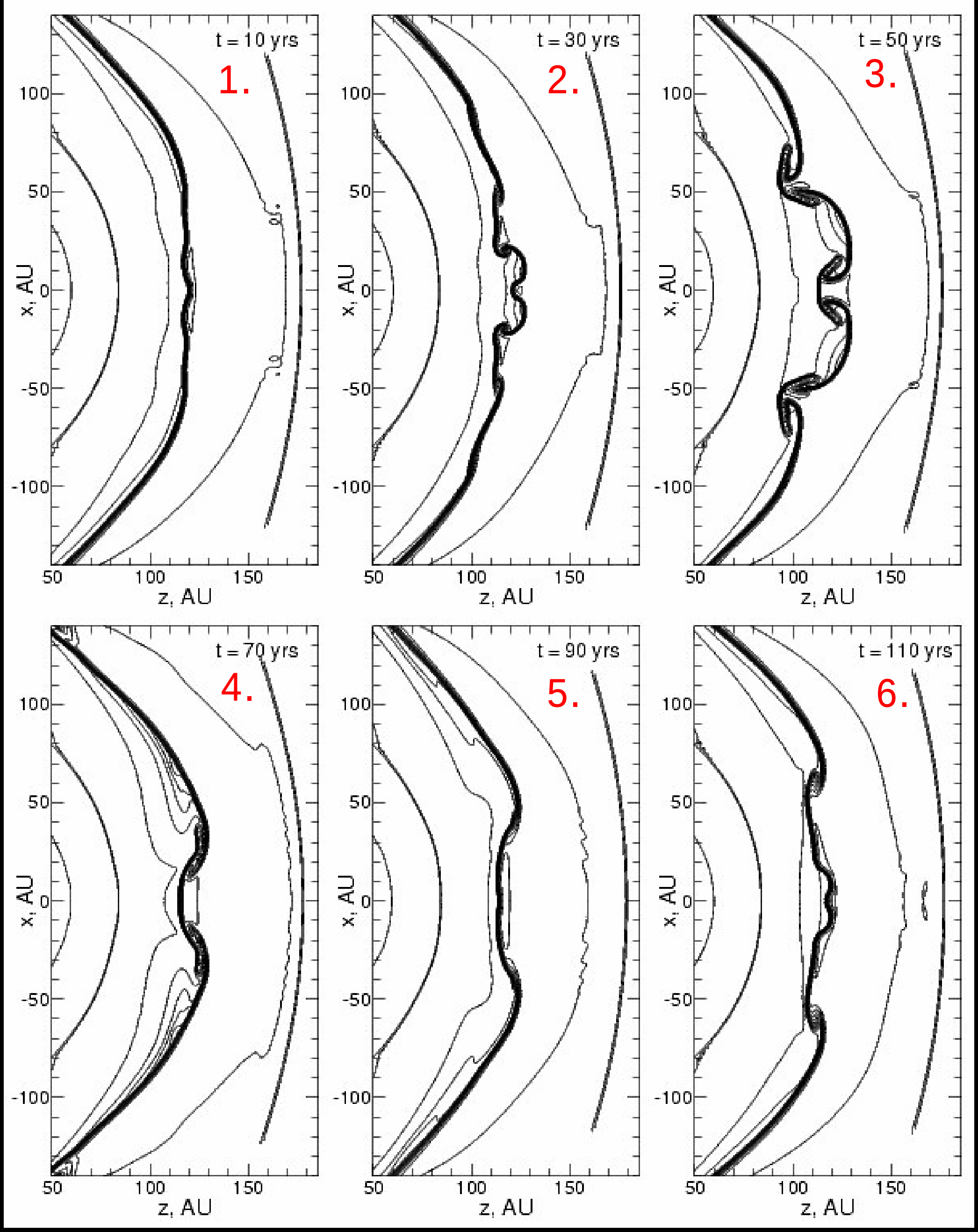

2-Fluid simulation

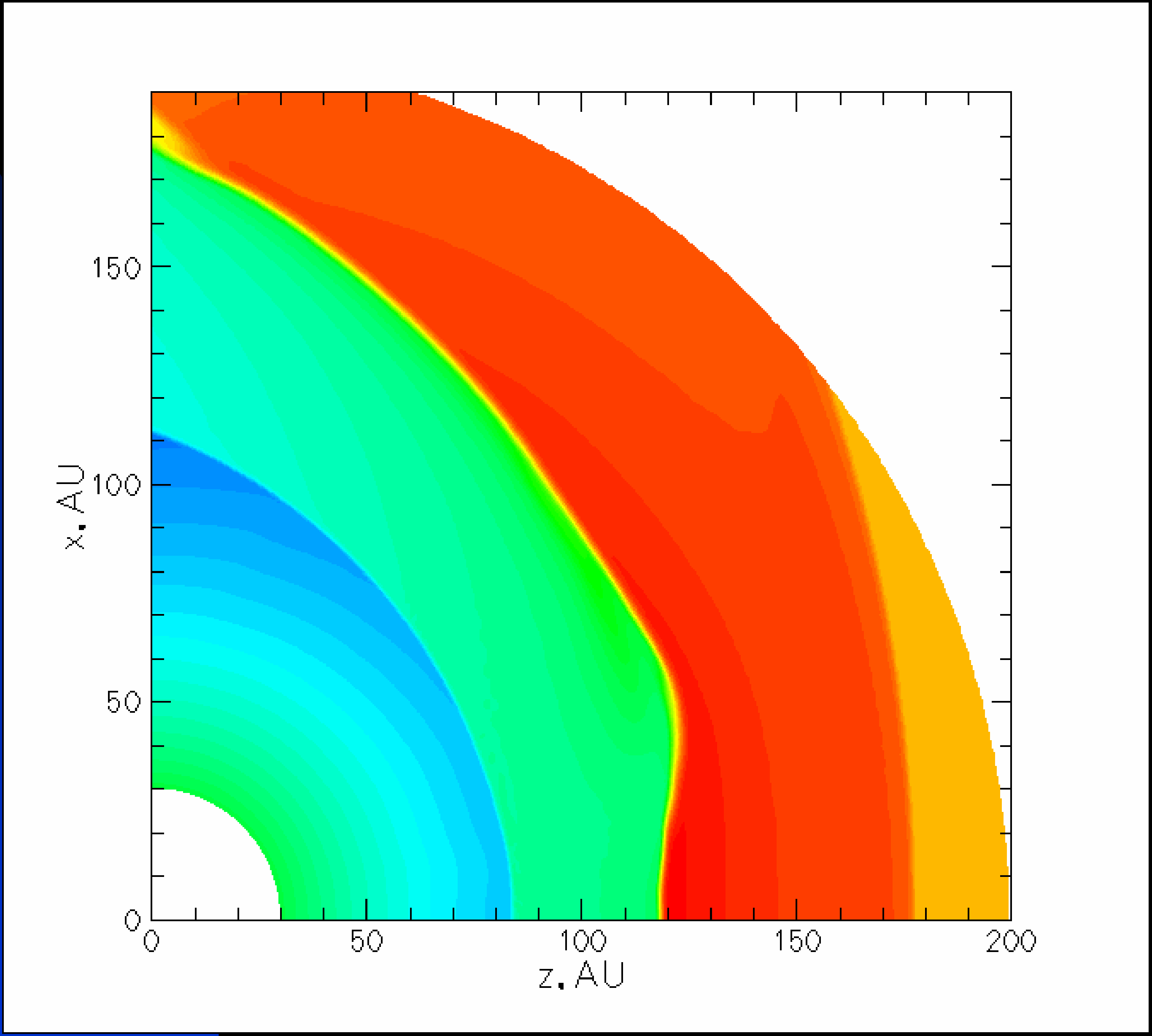

Dynamical Solar Wind-GMIRs

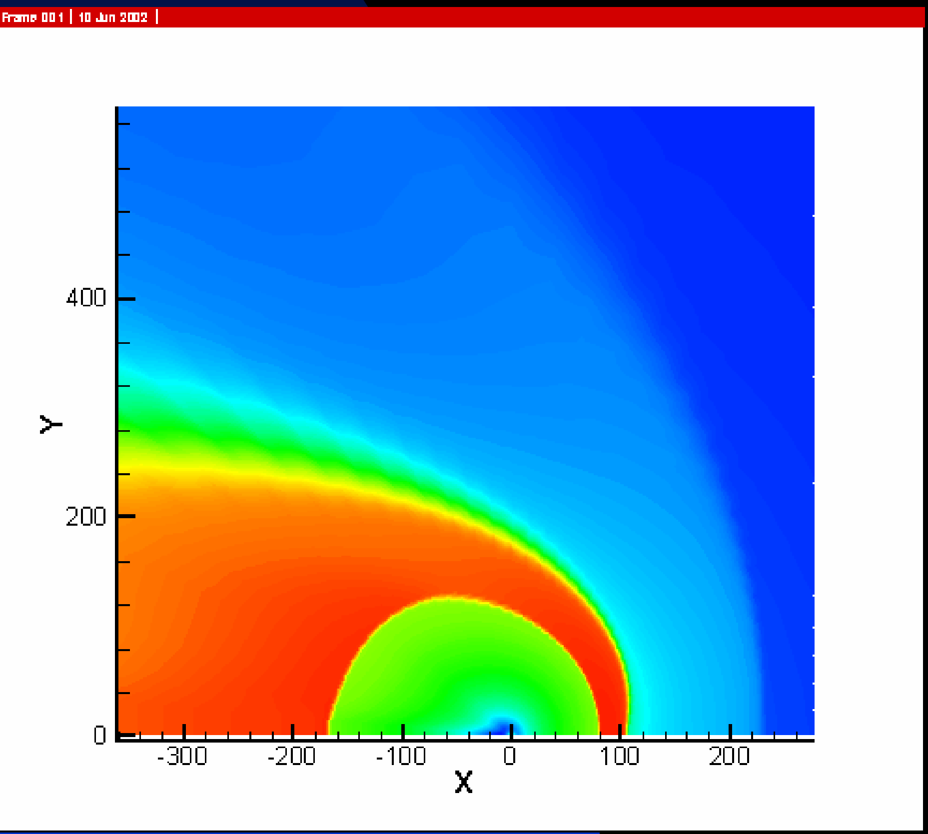

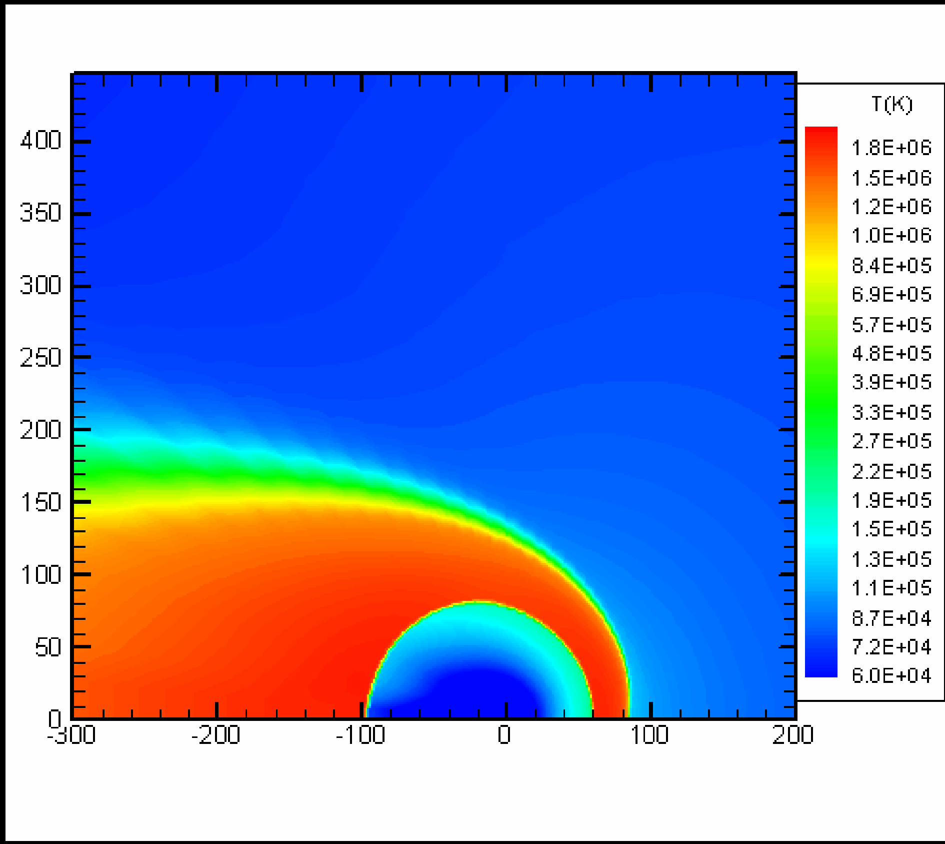

The physics of atom-plasma coupling

From perspective of QM, one cannot refer to outgoing proton as either being the initial H atom nucleus (i.e., a CE encounter) or simply the initial proton that scattered off the H atom – the two processes are indistinguishable.

- Need to consider total elastic cross-section for interaction of H and H^+

- Total cross-section much larger than usual CE only cross-section, but large proportion of collisions are small-angle.

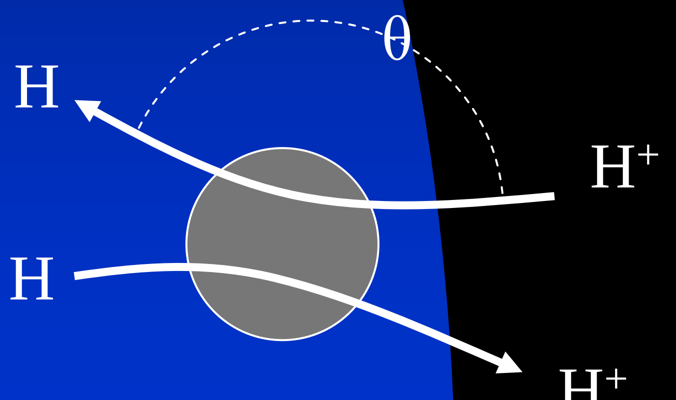

Charge exchange

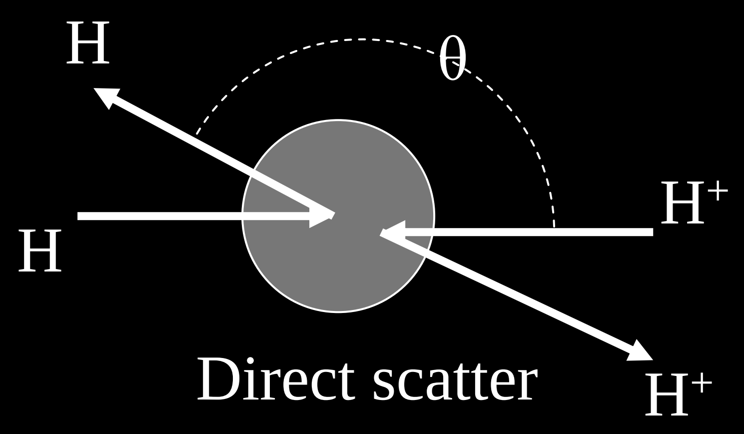

Direct scatter

The physics of atom-plasma coupling

From perspective of QM, one cannot refer to outgoing proton as either being the initial H atom nucleus (i.e., a CE encounter) or simply the initial proton that scattered off the H atom – the two processes are indistinguishable.

- Need to consider total elastic cross-section for interaction of H and H^+
- Total cross-section much larger than usual CE only cross-section, but large proportion of collisions are small-angle.

$$\boxed{H + H^+ \rightarrow H_2^+ \rightarrow H + H+}$$

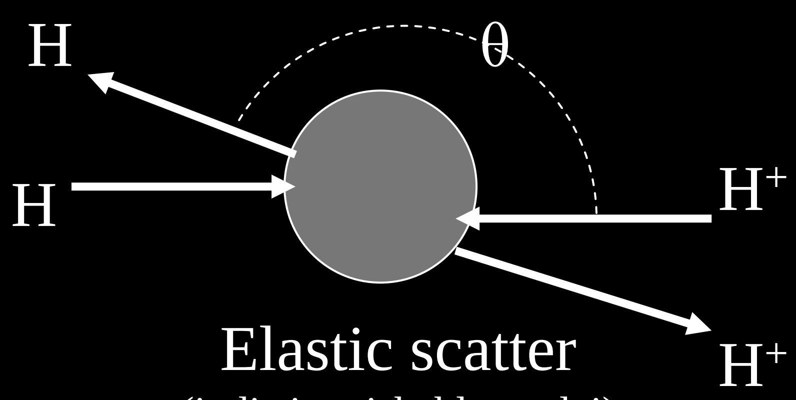

Elastic scatter
(indistinguishable nuclei)

The 3D Solar Wind

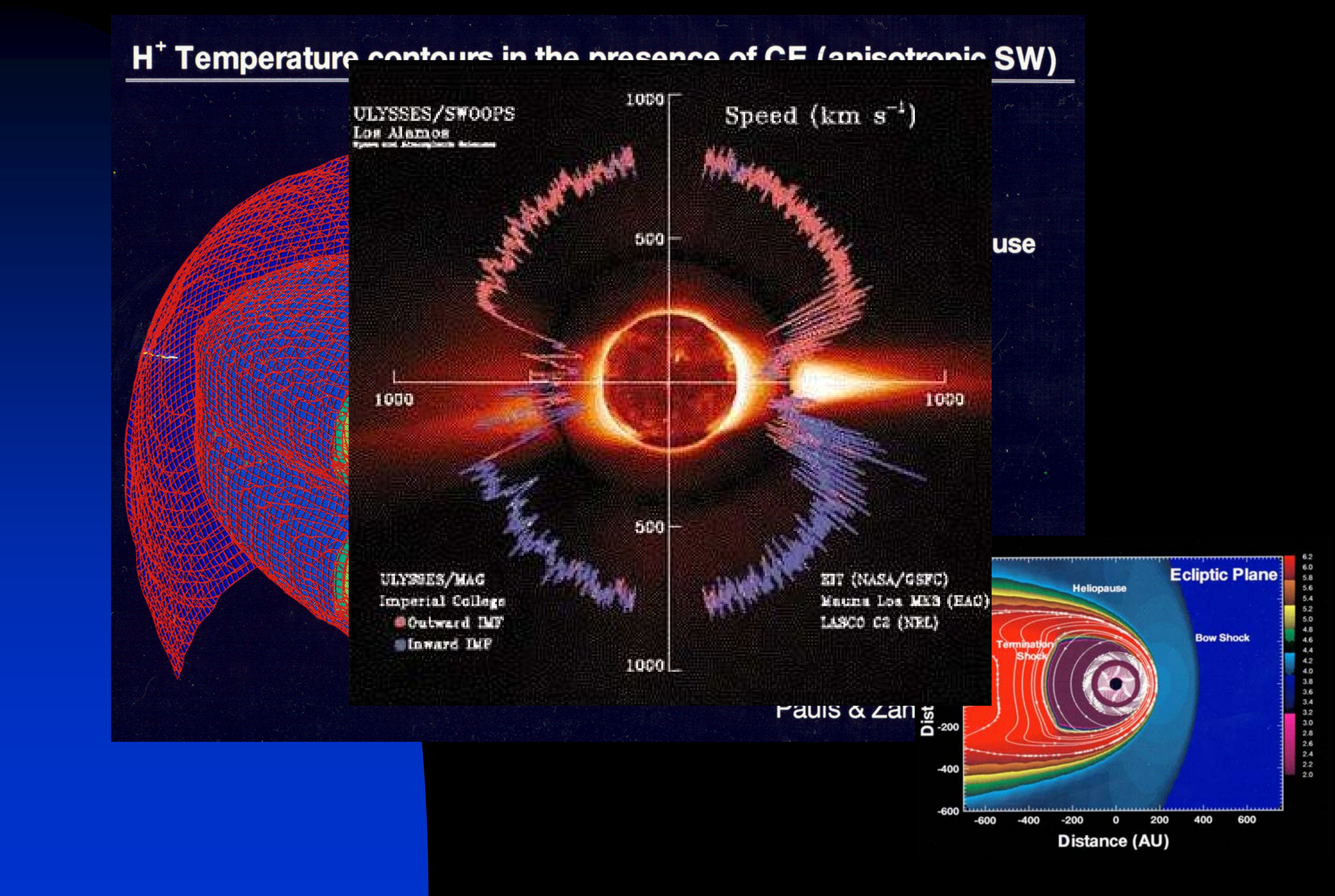

The Role of Interstellar Neutral H – 3D Models

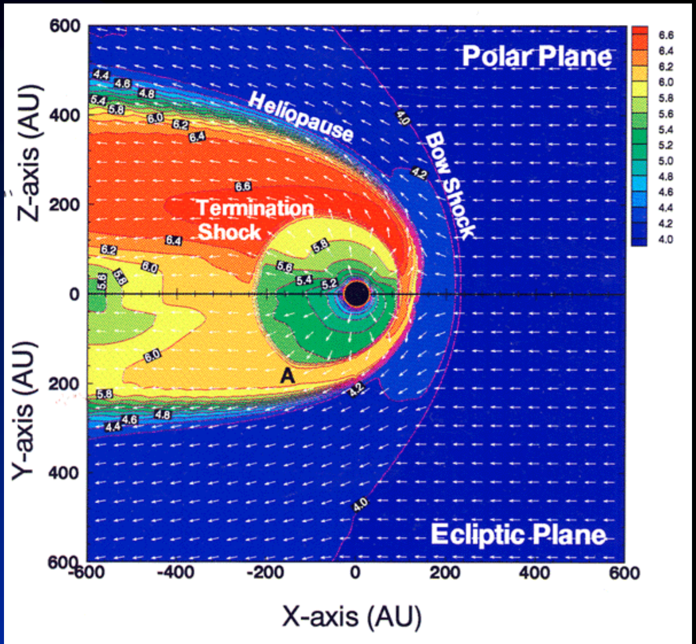

Plasma temperature

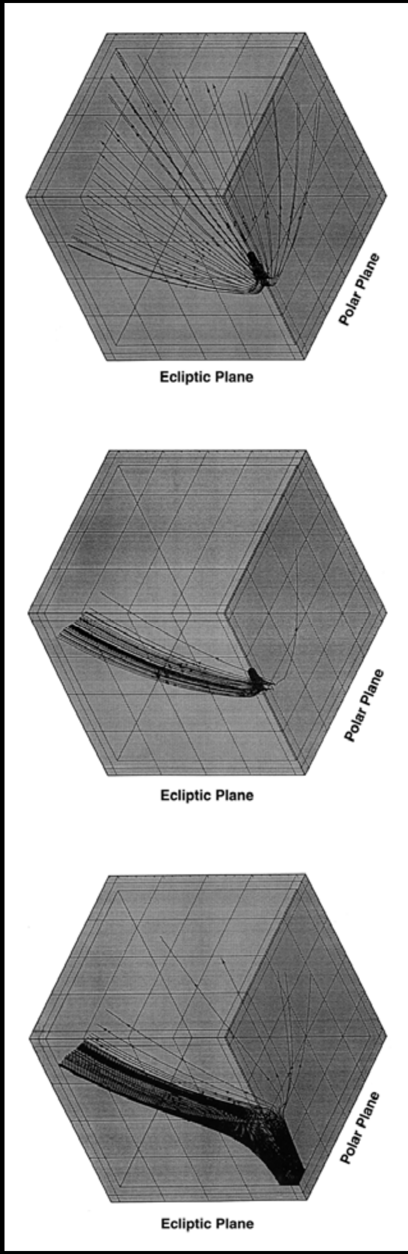

Neutral density

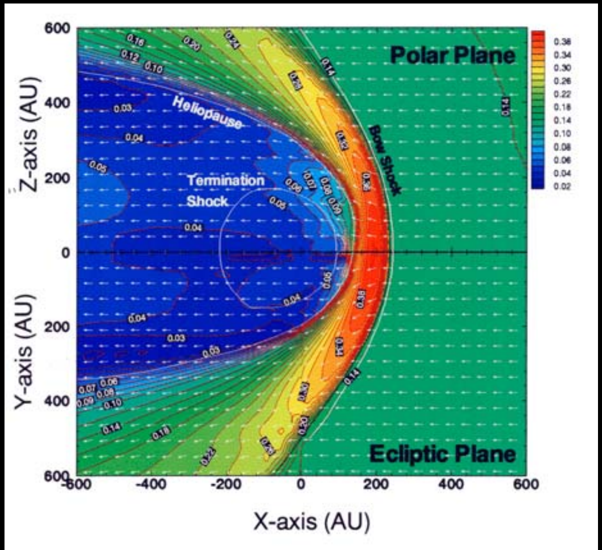

Three-dimensional structure of the heliosphere in the presence of the IMF and ISMF

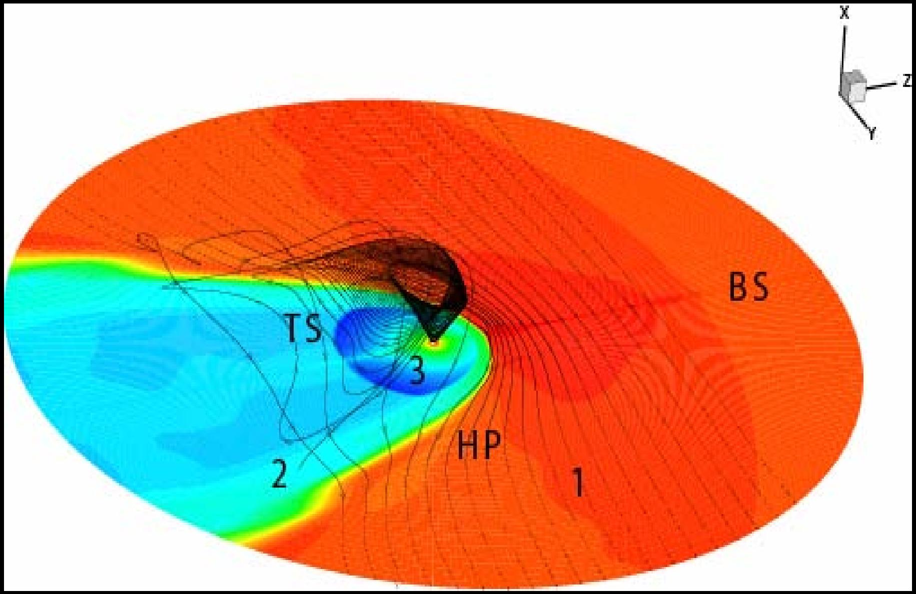

We assume that the SW is spherically symmetric at the inner boundary and initially set V_p = 450 km/s, n_p = 7 cm^{-3}, and T_p = 73600 K.

In the LISM we put V_∞ = 25 km/s, n_∞ = 0.07 cm^{-3}, M_∞ = 2, $n_{H\infty}$ = 0.1 cm^{-3}, and B_∞ = 1.5 μG. The direction of the ISMF is not well known and remains a parameter of the problem.

The importance of neutral atoms

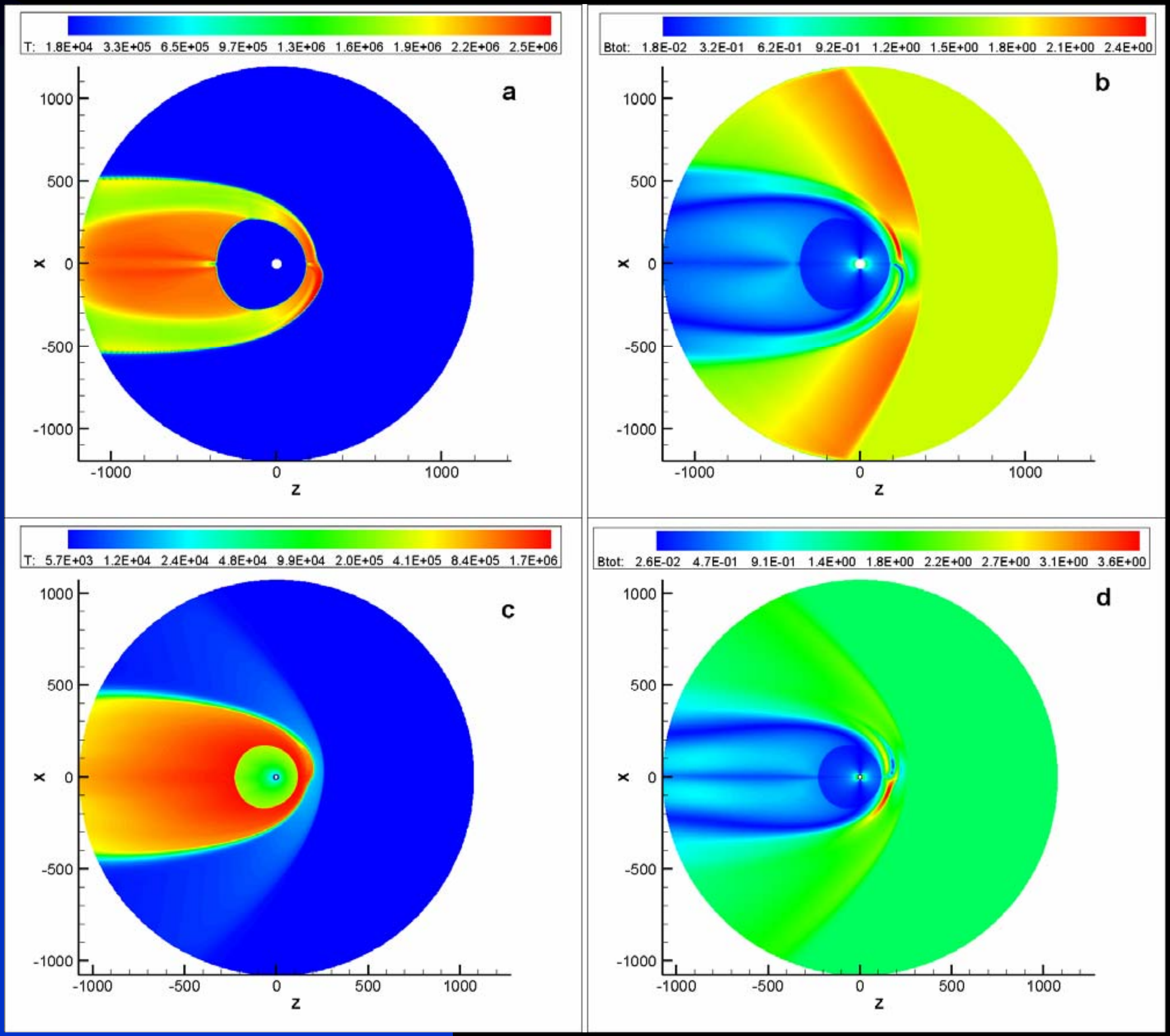

ISMF parallel to the LISM velocity: without neutrals (a, b) and with neutral hydrogen atoms (c, d).

Multi-fluid modeling of the SW-LISM interaction

HCS instabilities due to charge exchange

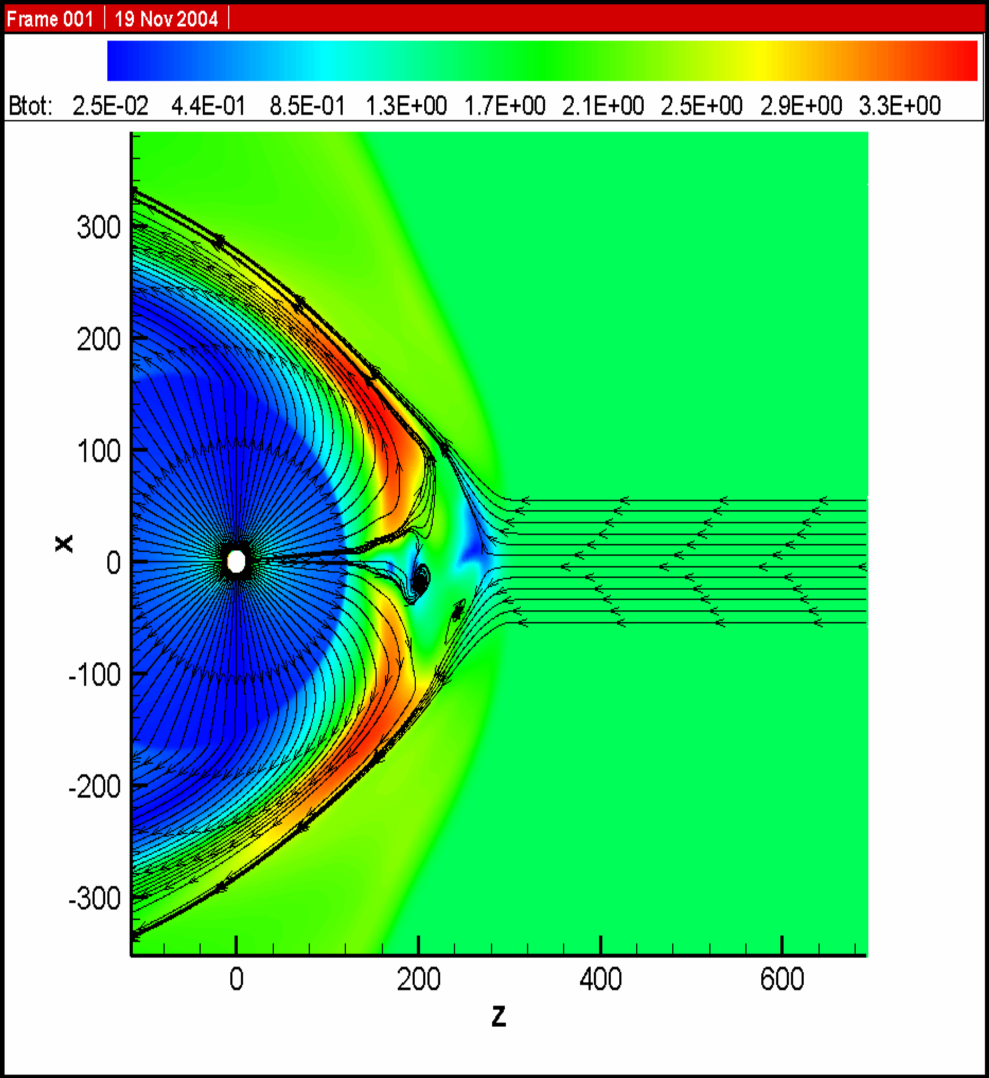

Magnetic field magnitude distribution in the meridional plane

ISMF perpendicular to the LISM velocity vector and Sun's rotation axis

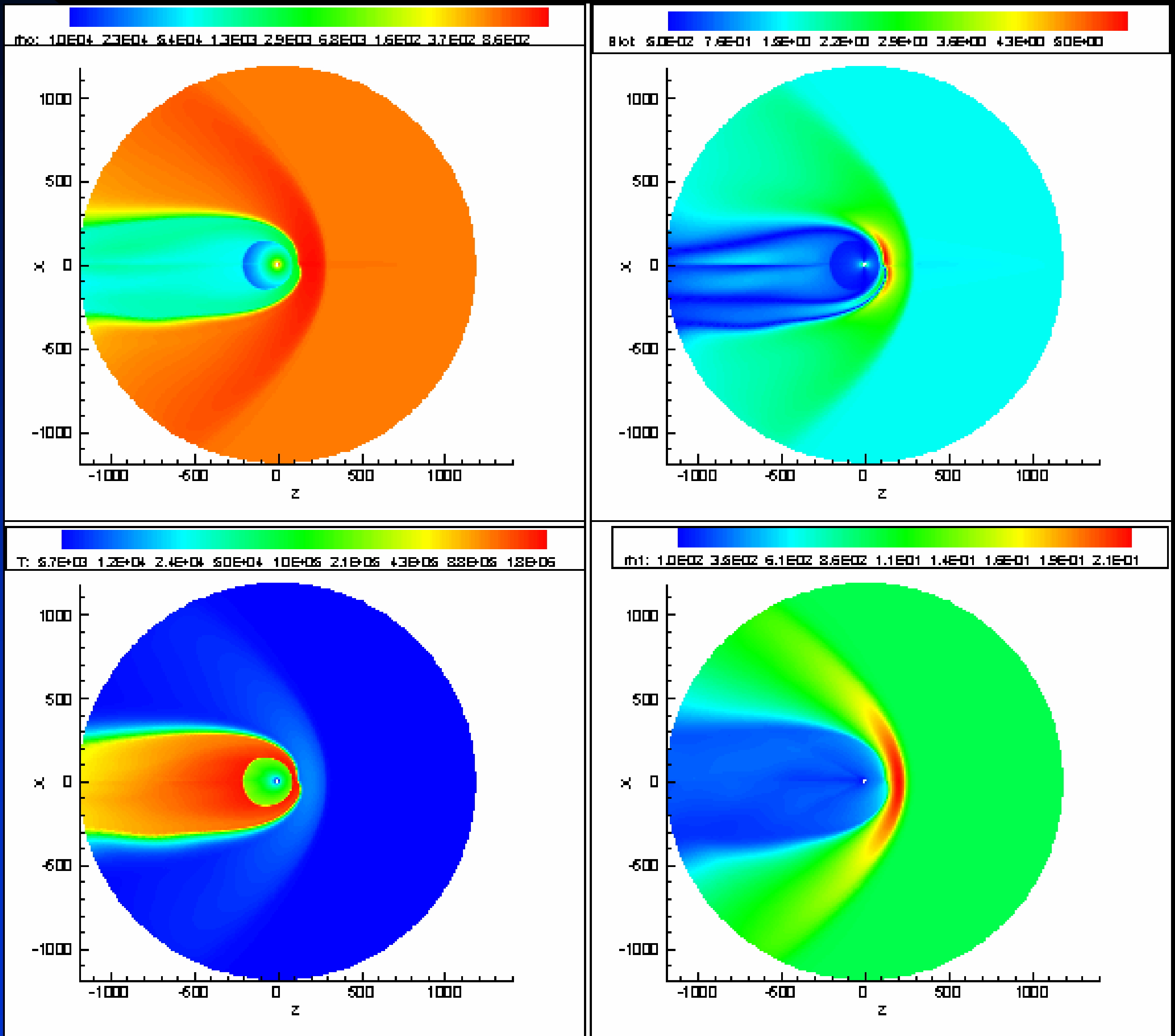

B_∞ = 1.5 μG, that is, LISM flow is superfast.

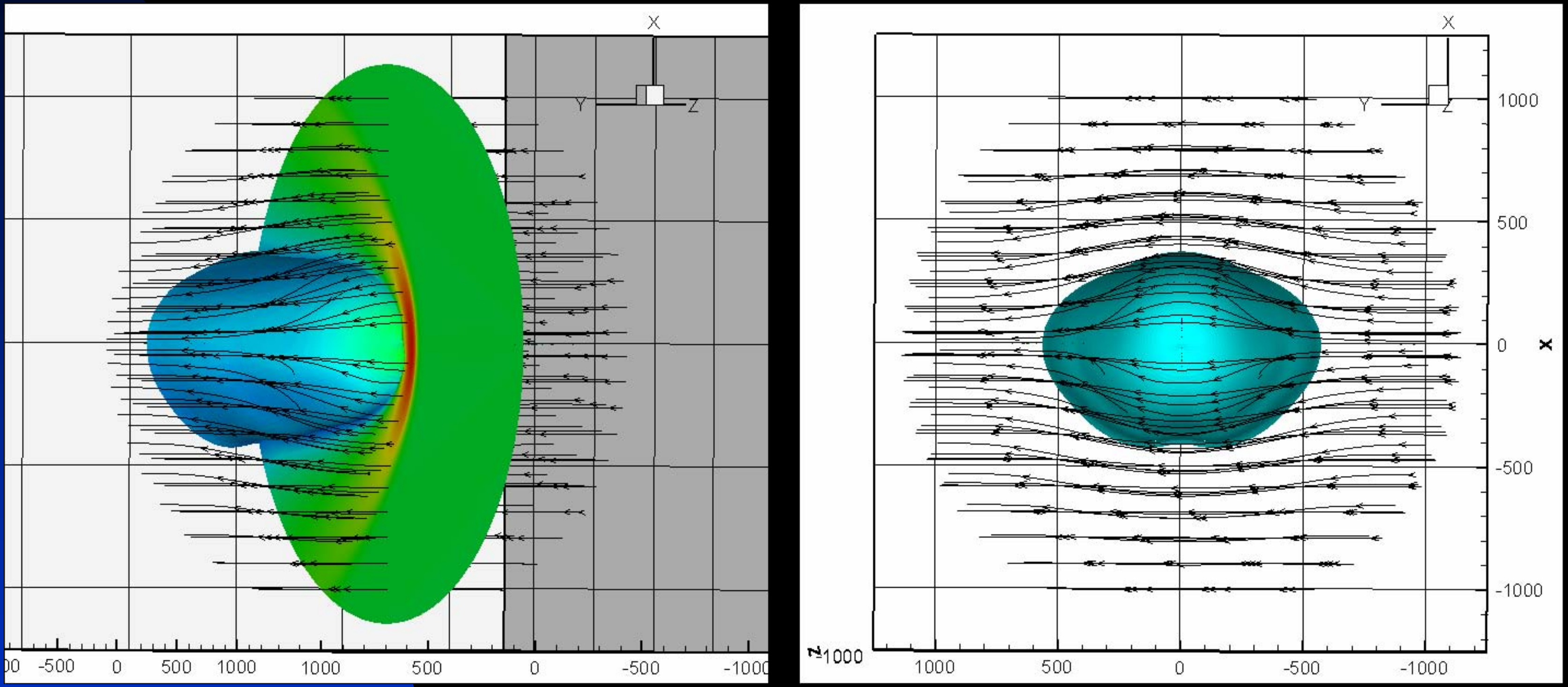

Side and front views of the heliopause draped by the ISMF lines

The angle between the ISMF and the LISM velocity is 45°

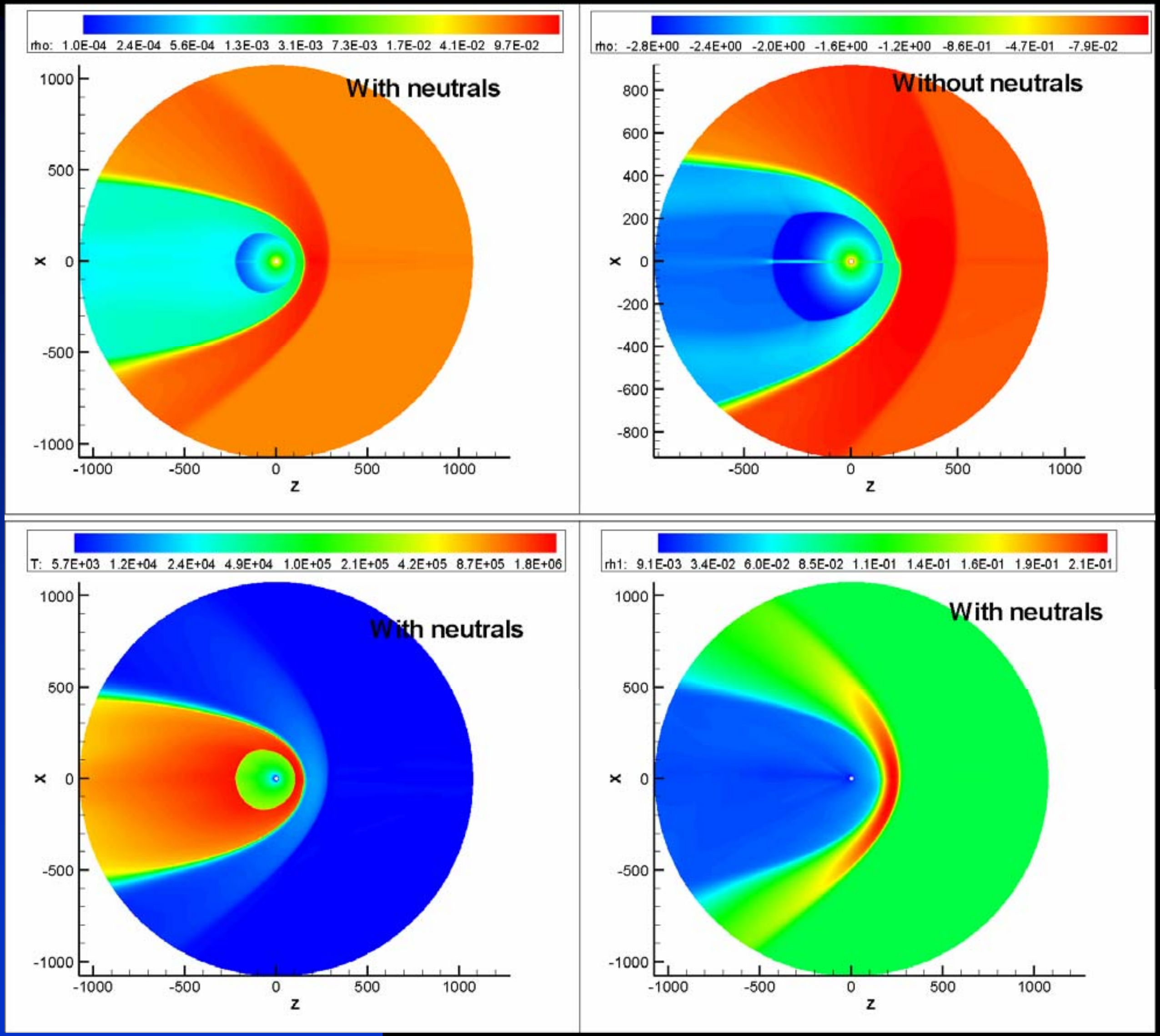

Asymmetry of discontinuities with respect to the ecliptic plane become considerably less pronounced!

ISMF perpendicular to the LISM velocity and tilted 60° to the ecliptic plane.

Cross-sections of the widest and narrowest flaring of the heliopause

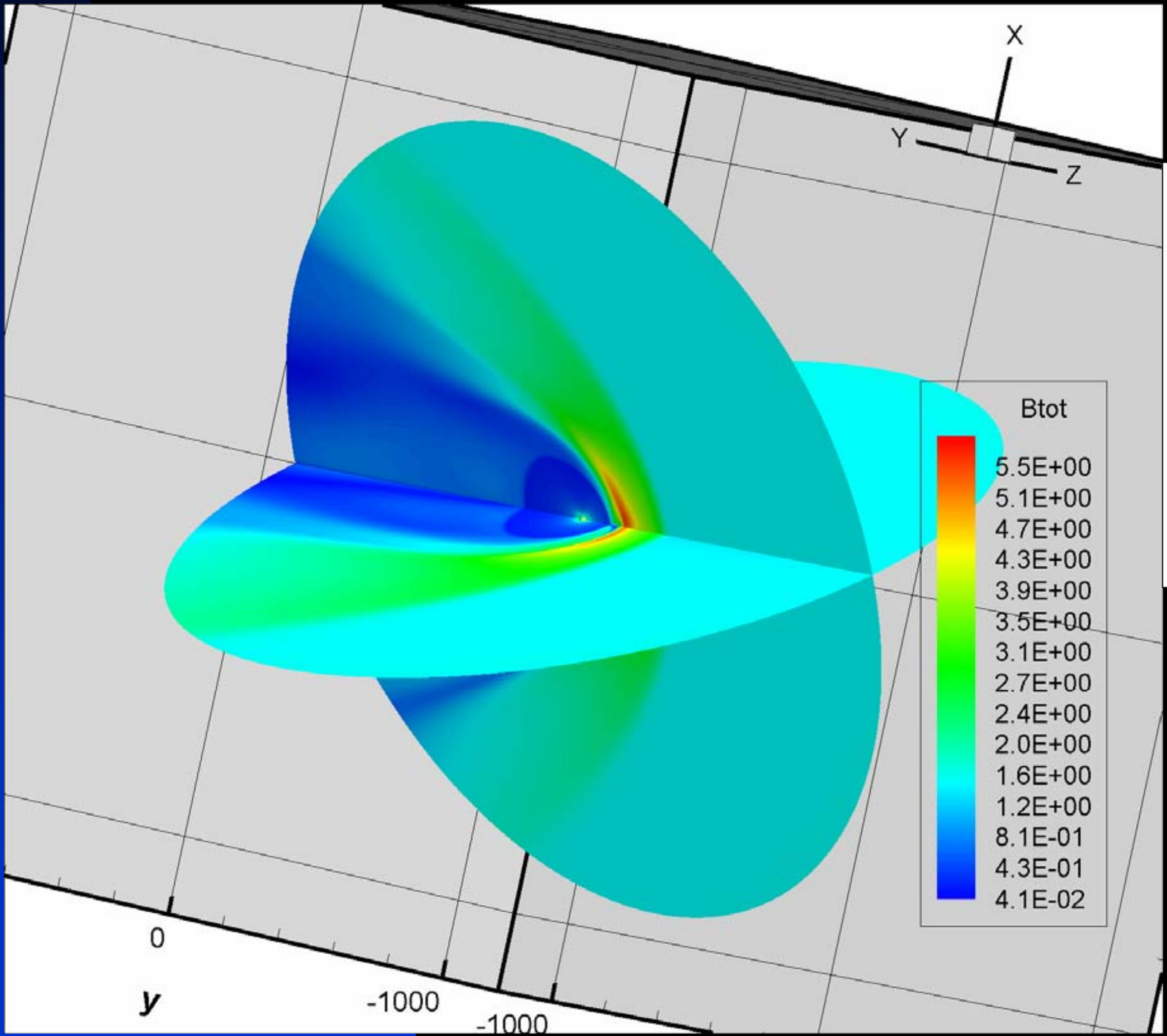

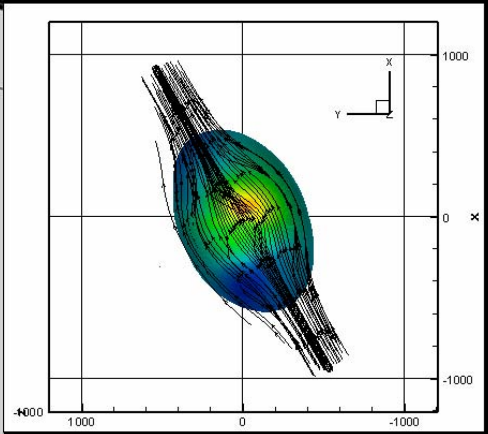

Comparison of MHD, 2-fluid, and 4-fluid models

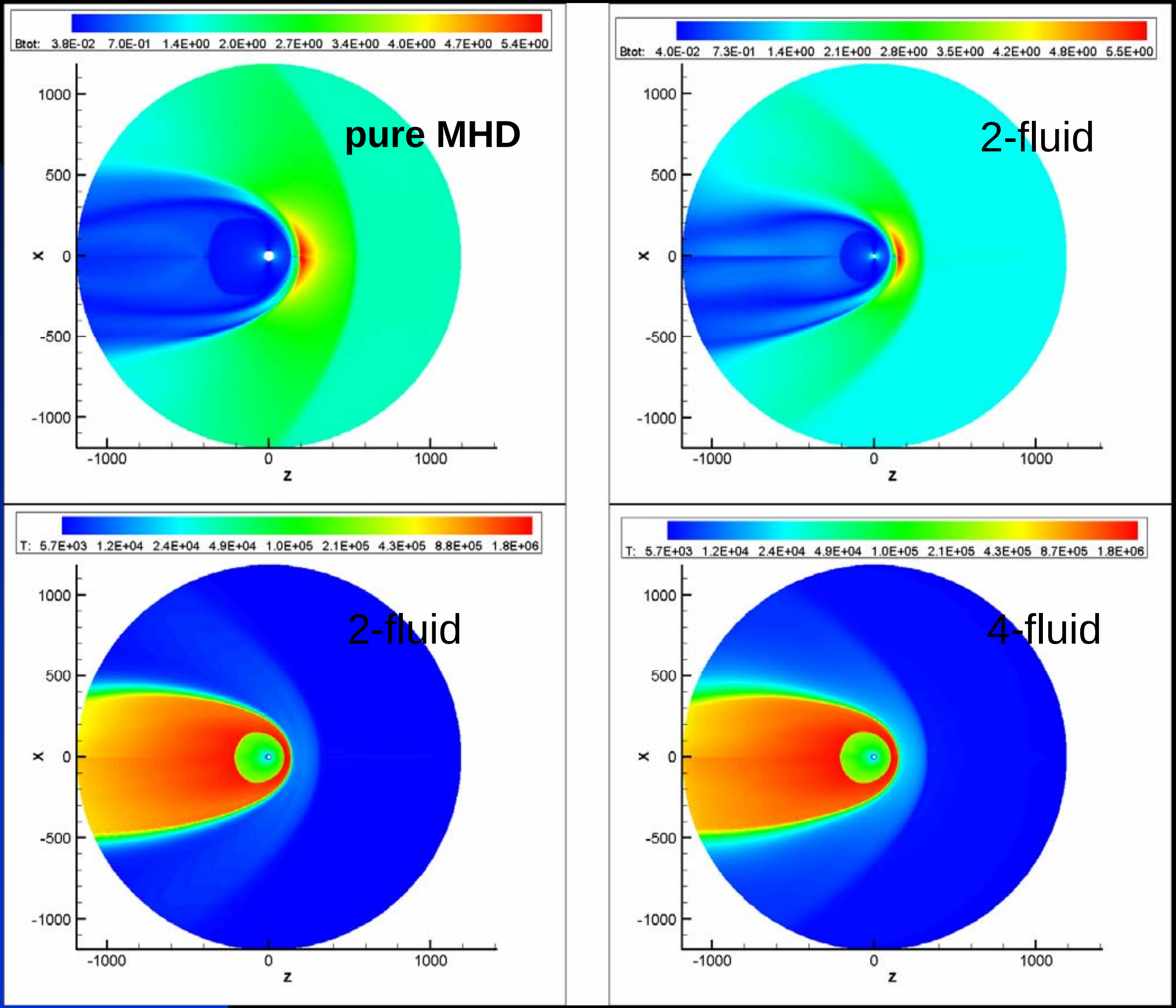

HCS bending and rotation

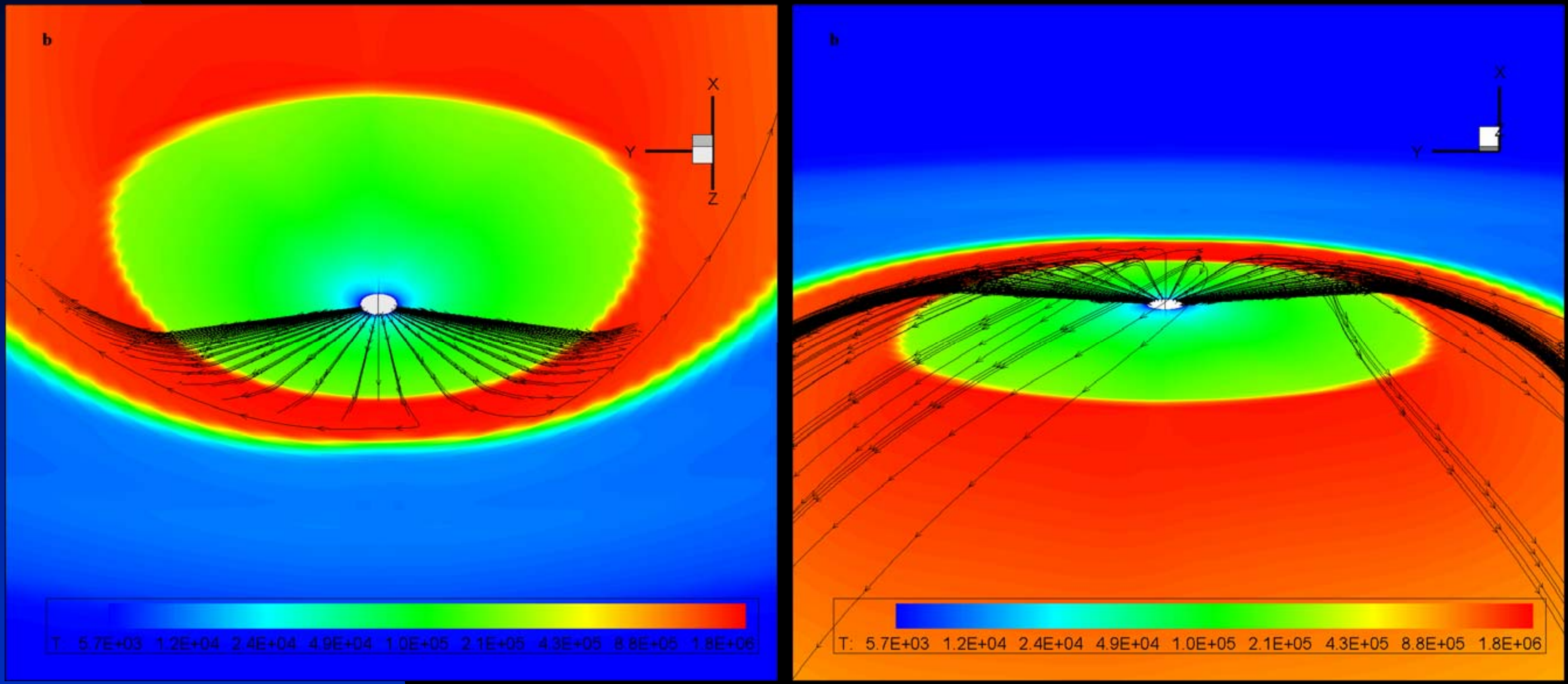

SW streamlines starting above the ecliptic plane
(views from above and below the ecliptic plane)

V-shaped grooves on the surface of the heliopause (boundary conditions for the HCS)

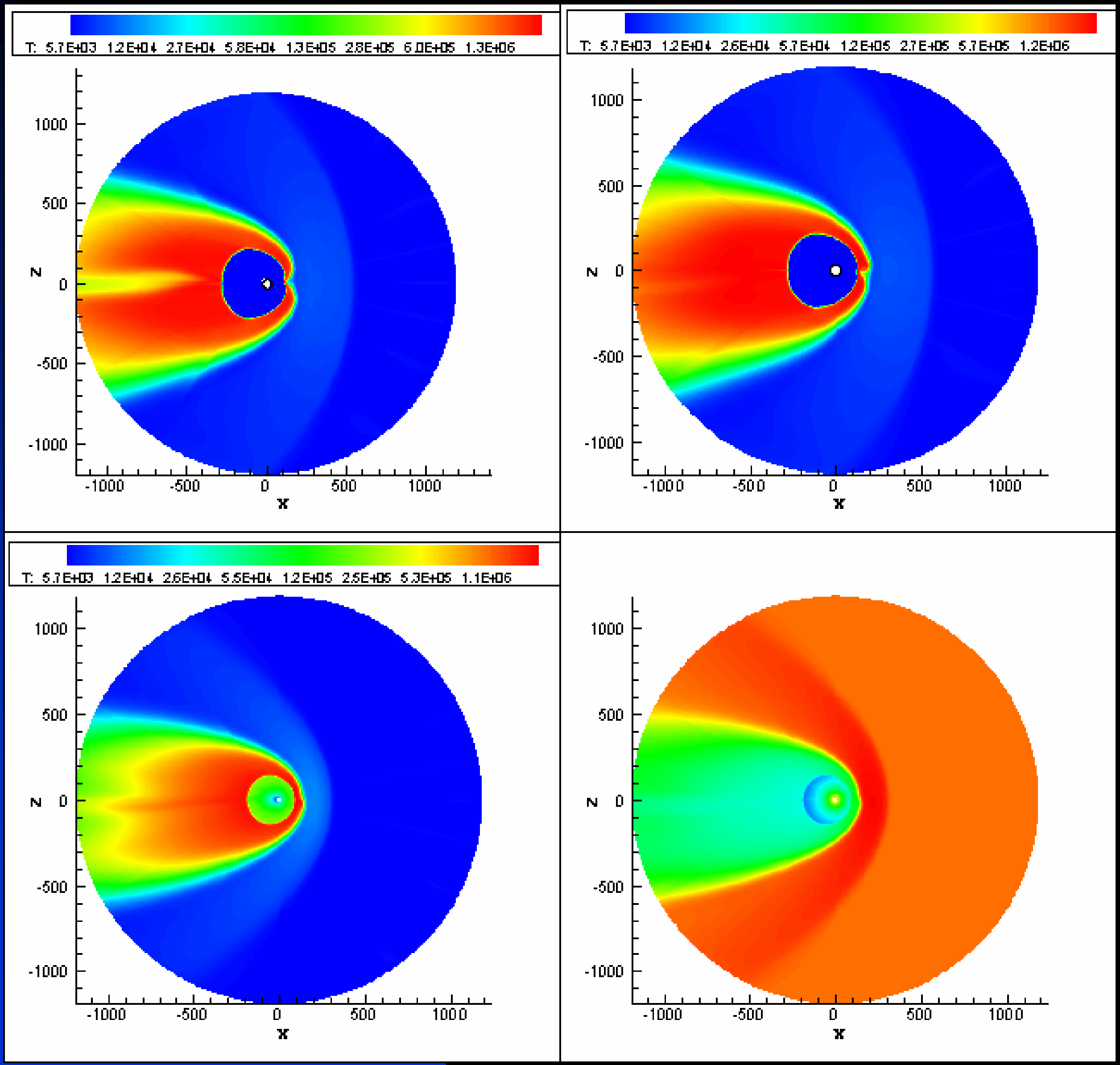

(a) and (b) temperature distributions without H-atoms and with magnetic field eliminated in the 0.75°- and 0.375°- sectors symmetric with respect to the ecliptic plane.
(c) and (d) plasma temperature and density in the presence of neutral atoms.

On the possibility of multiple crossing of the termination shock by IMF lines

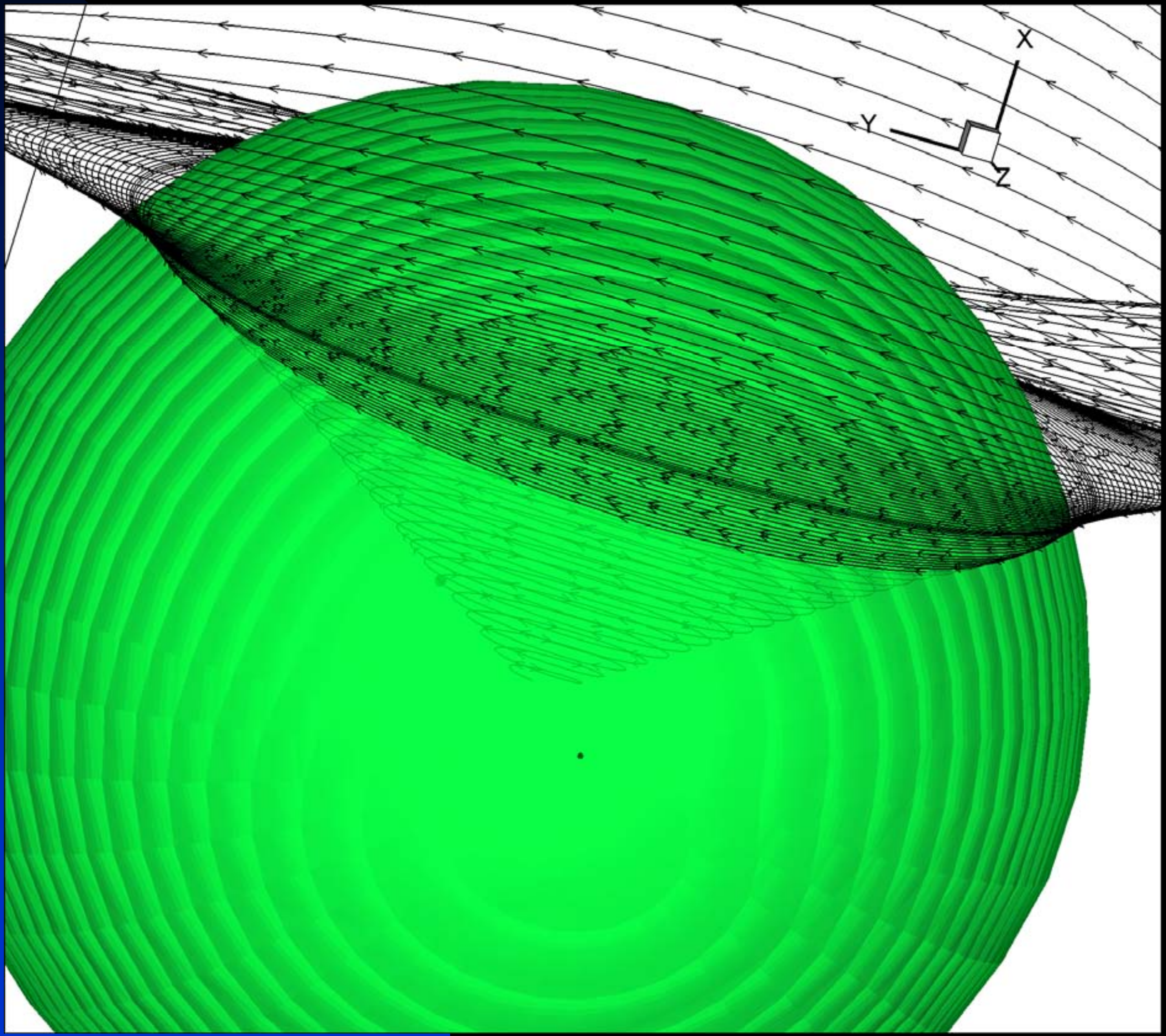

Energetic charged particle latitudinal streaming anisotropy data can be explained by multiple crossing of the termination shock by IMF lines (Jokipii et al, 2004). The possibility of such crossings was discussed by Zank (1999). Here we show one of the calculated IMF lines that crosses the termination shock approximately at the Voyager 1 location.

The angle between the LISM H and He velocity vectors (LISM stagnation point displacement with respect to the ecliptic plane)

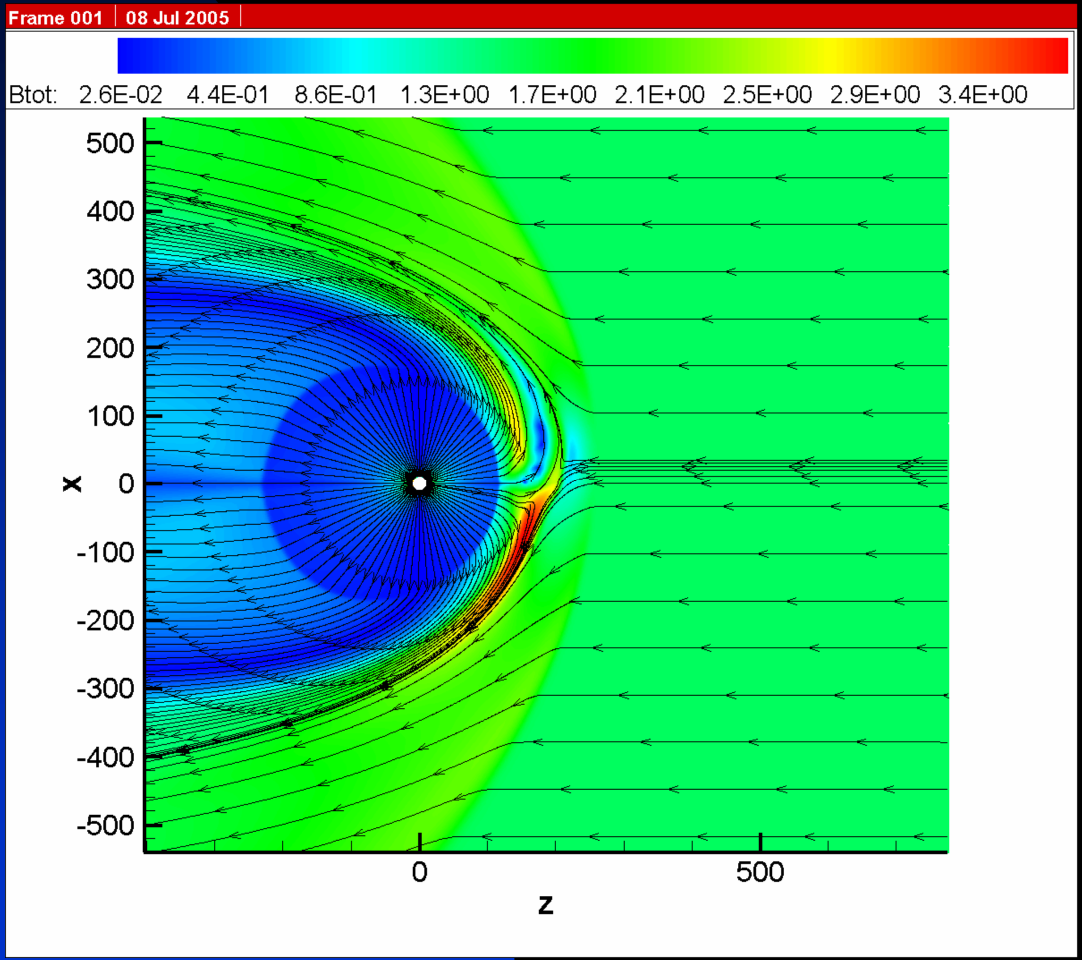

Lallement et al. (2005) determined an angle ≈ 4° between the He and H velocity vectors. A possible reason is a displacement of the LISM stagnation point with respect to the ecliptic plane (Izmodenov et a., 2005, who considered a 45° angle between V_∞ and B_∞ and neglected the influence of the IMF).

LISM velocity parallel to the interstellar magnetic field vector (B_∞ = 1.5 μG):

displacement ~ 5°!

H-atoms streamlines

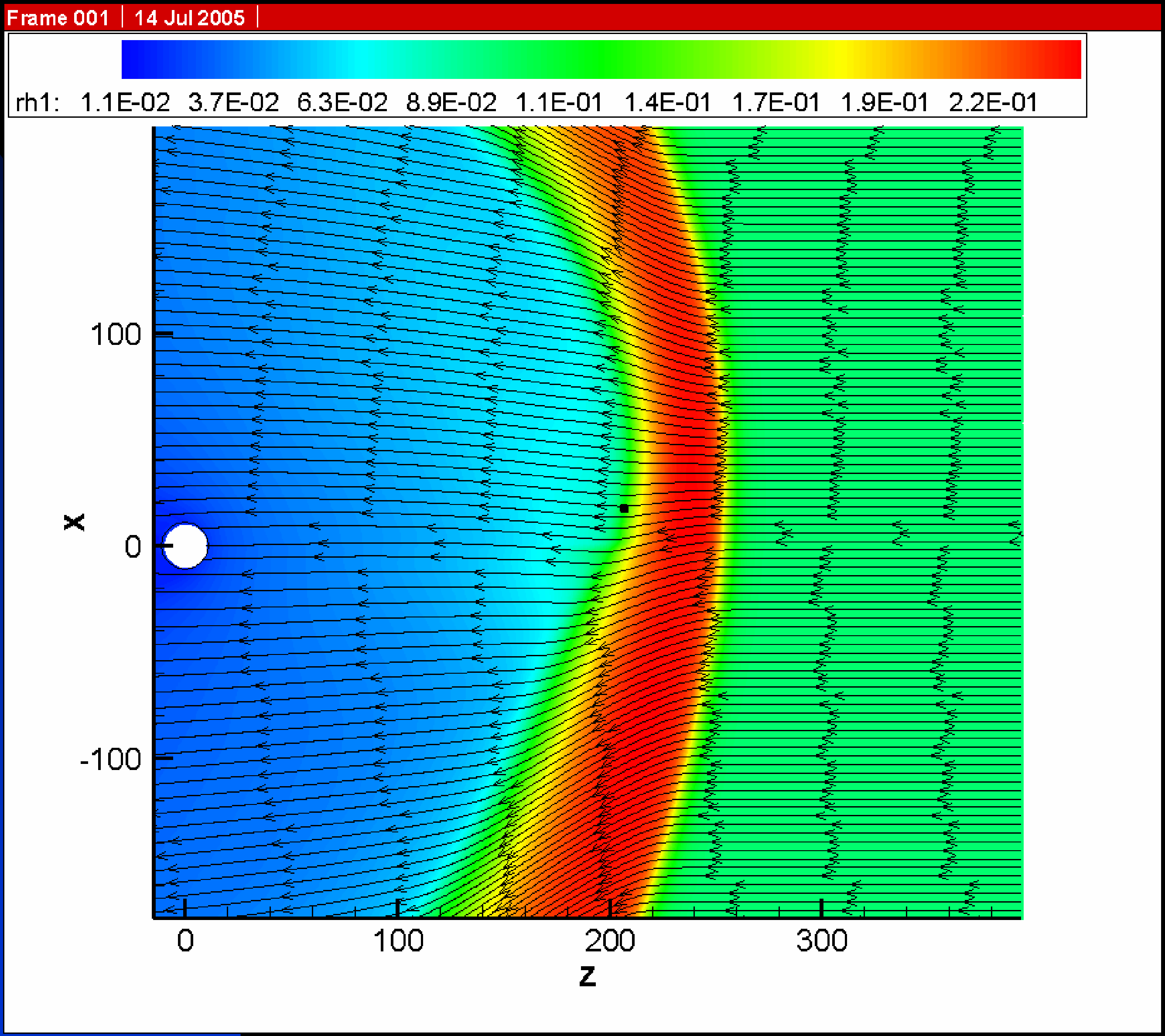

MHD CONCLUSIONS

1. 3D calculations of the SW-LISM interaction taking into account interplanetary and interstellar magnetic fields, and neutral hydrogen included using multi-fluid approach. Bending of the HCS is likely for most of the ISMF orientations.

2. Certain orientations of the interstellar magnetic field with respect to the LISM velocity and the solar ecliptic plane create asymmetric magnetic pressure distributions at the outer side of the heliopause - might explain of the observed distribution of radio emission sources in that region.

3. The IMF lines can exhibit multiple crossings of the termination shock and repeatedly penetrate from the supersonic SW region into the heliosheath.

4. Analysis of solutions for various ISMF strengths and directions with respect to the LISM velocity shows that small deviations between the He- and H-streams reported by Lallement et al. (2005) can be obtained for many different orientations of B.

Large step decreases in the CR modulation cycle are coupled to GMIRs, which are mainly associated with systems of transients near the Sun. The transient streams merge in such a way that beyond ~ 20 AU large-scale GMIRs form from overlapping MIRs which persist over several solar rotations, surround the Sun near the ecliptic plane, and extend to at least 30° in heliolatitude above the equatorial plane (Burlaga, 1993) .

Consider the interaction of a steady-state heliosphere with a model spherically symmetric perturbation in the SW velocity, which increases 3 times within 60 days and then returns to its initial value after another 60 days.

$$U(t) = 18 \times \left\{ 1 + 2.1 \exp\left[-\left(\frac{t - 1.864}{0.57} \right)^2 \right] \right\}$$

Magnetic field distribution caused by the GMIR propagation

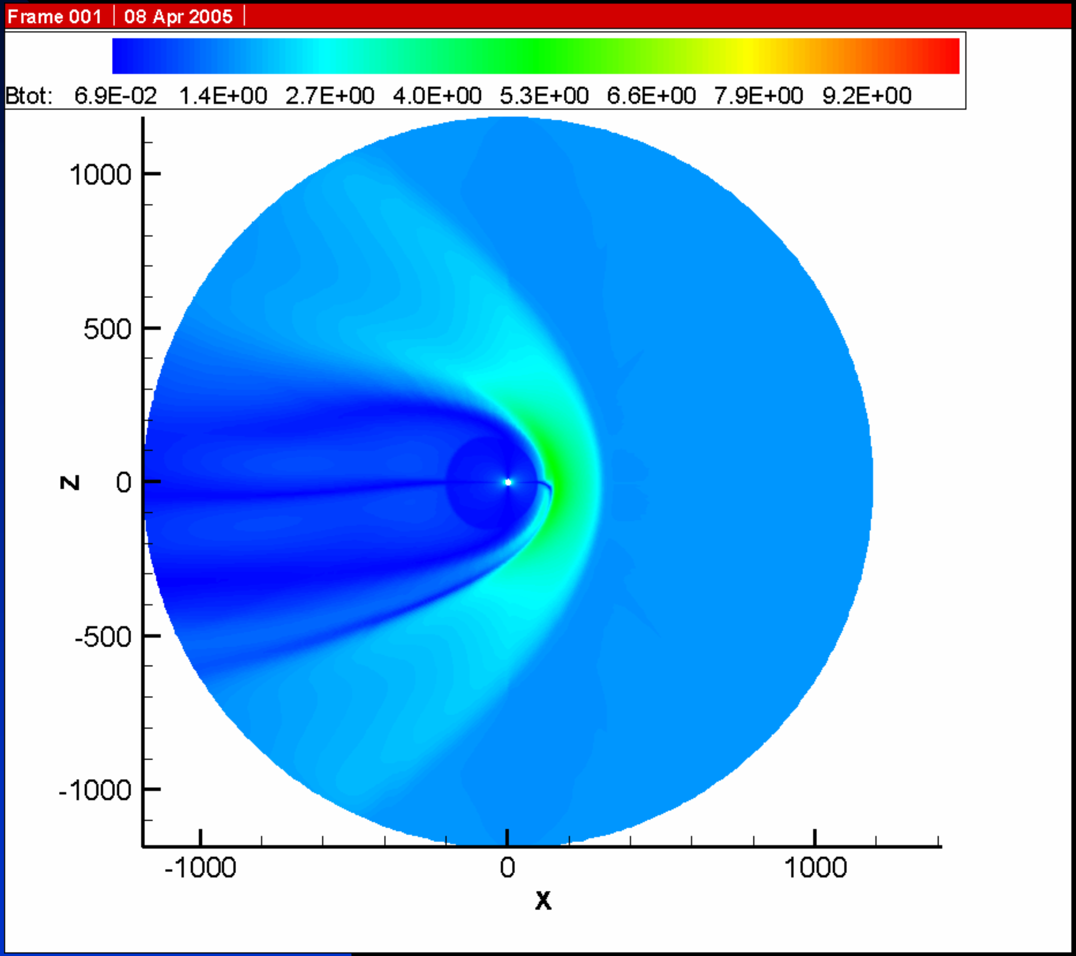

Frames 1-25:

sequence of snapshots at t=0,

66.5,
121.7,
154.6,
179.5,
206.9,
242.7,
292.6,
346.2,
400,
and 457.5 days.

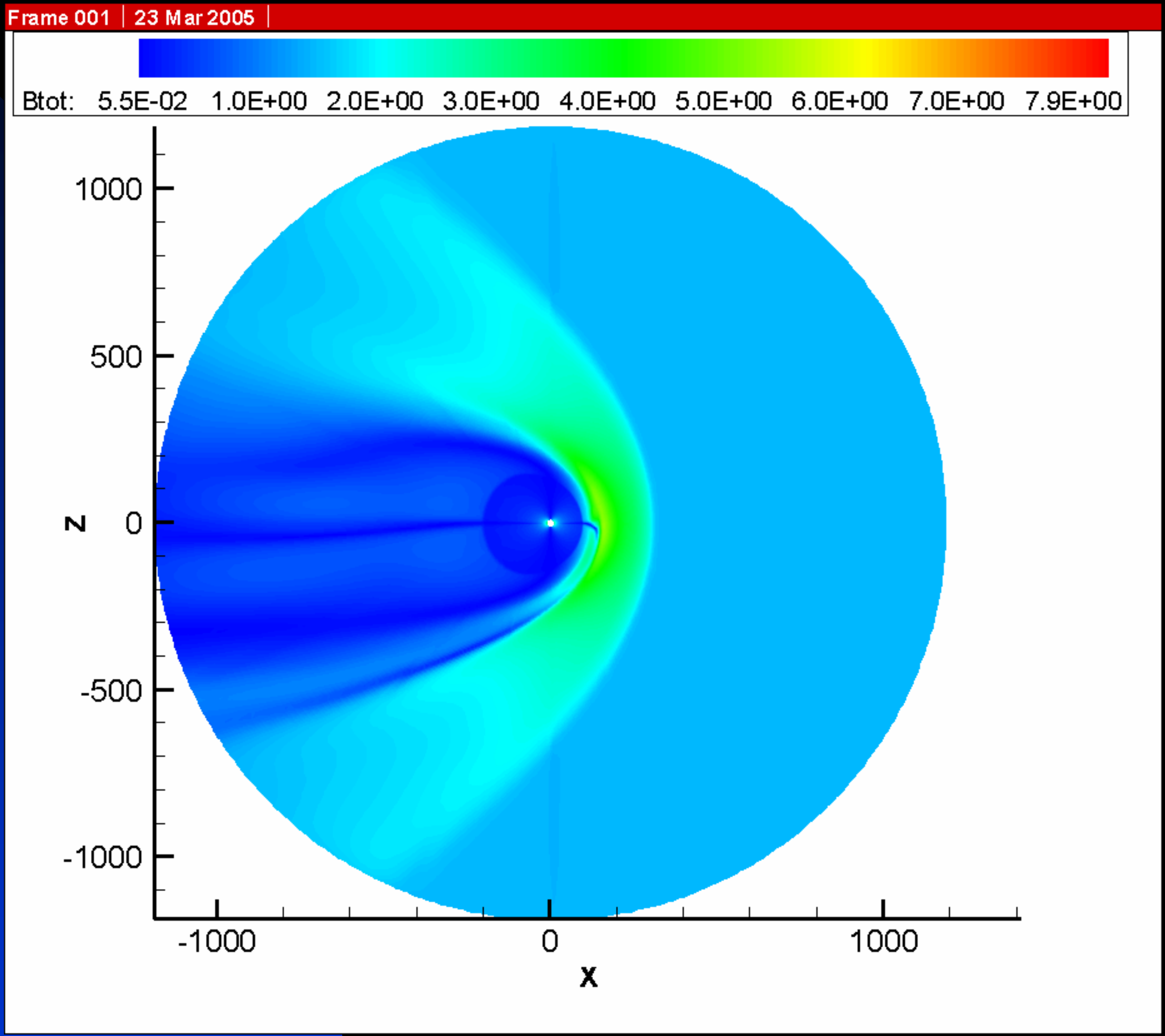

The first 25 frames at twice larger interval

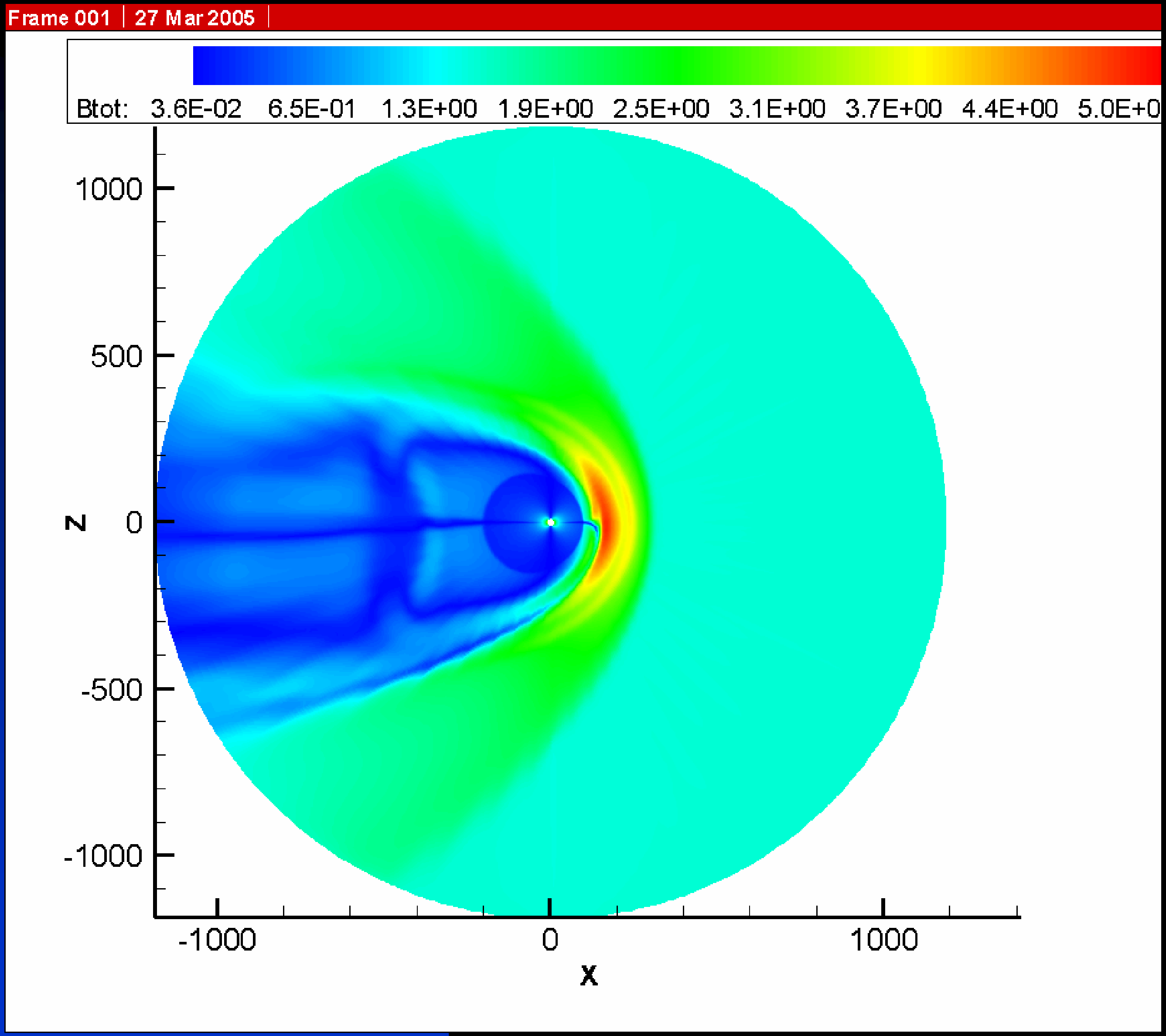

The next 50 time steps.

Magnetic field scaling is different from the previous two slides!

Density distributions

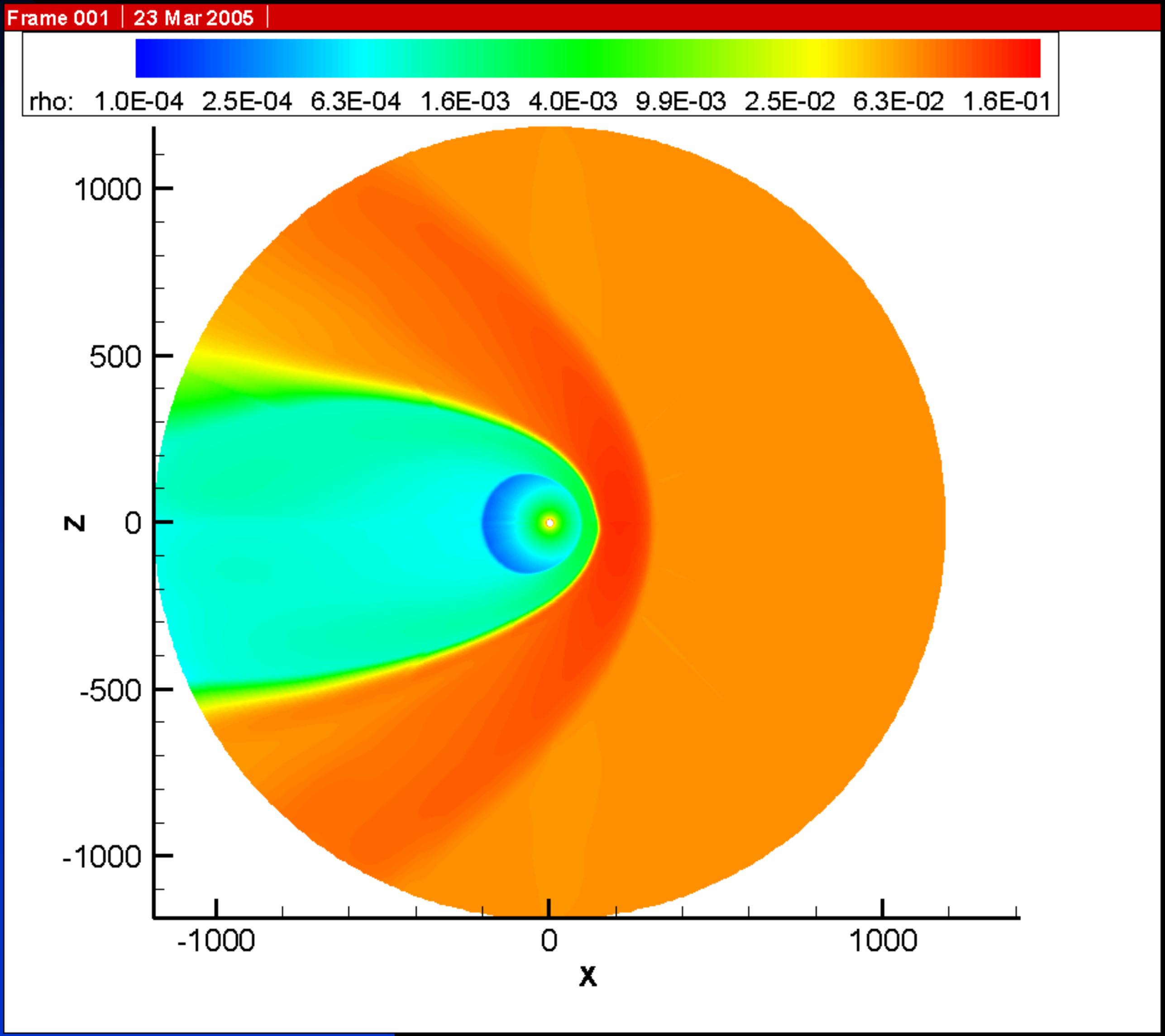

Frames 1-25

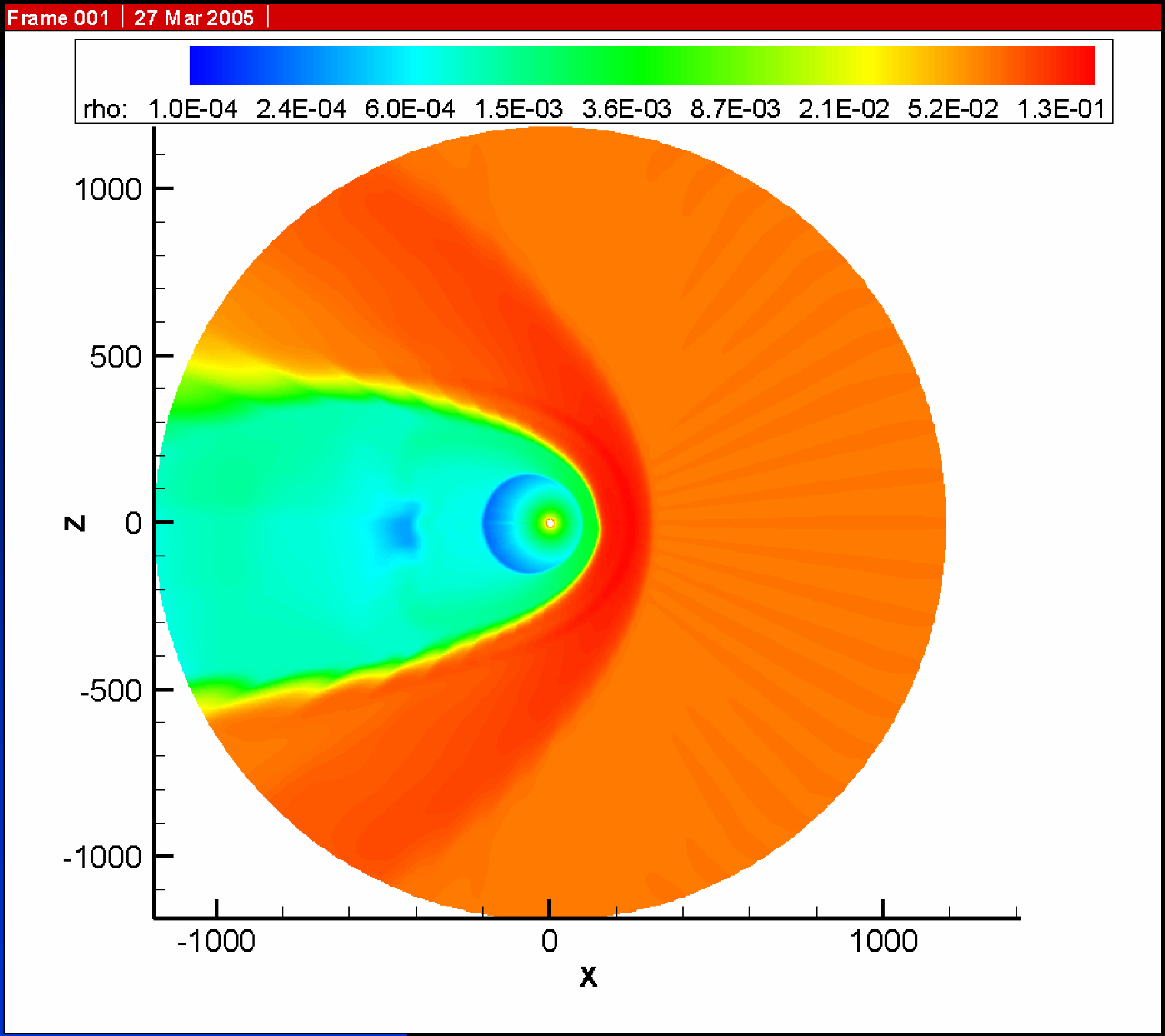
Frame 001 | 27 Mar 2005
rho: 1.0E-04 2.4E-04 6.0E-04 1.5E-03 3.6E-03 8.7E-03 2.1E-02 5.2E-02 1.3E-01
1000
500
0
-500
-1000
Z
-1000
0
1000
X

Frames 26-55

Temperature distributions

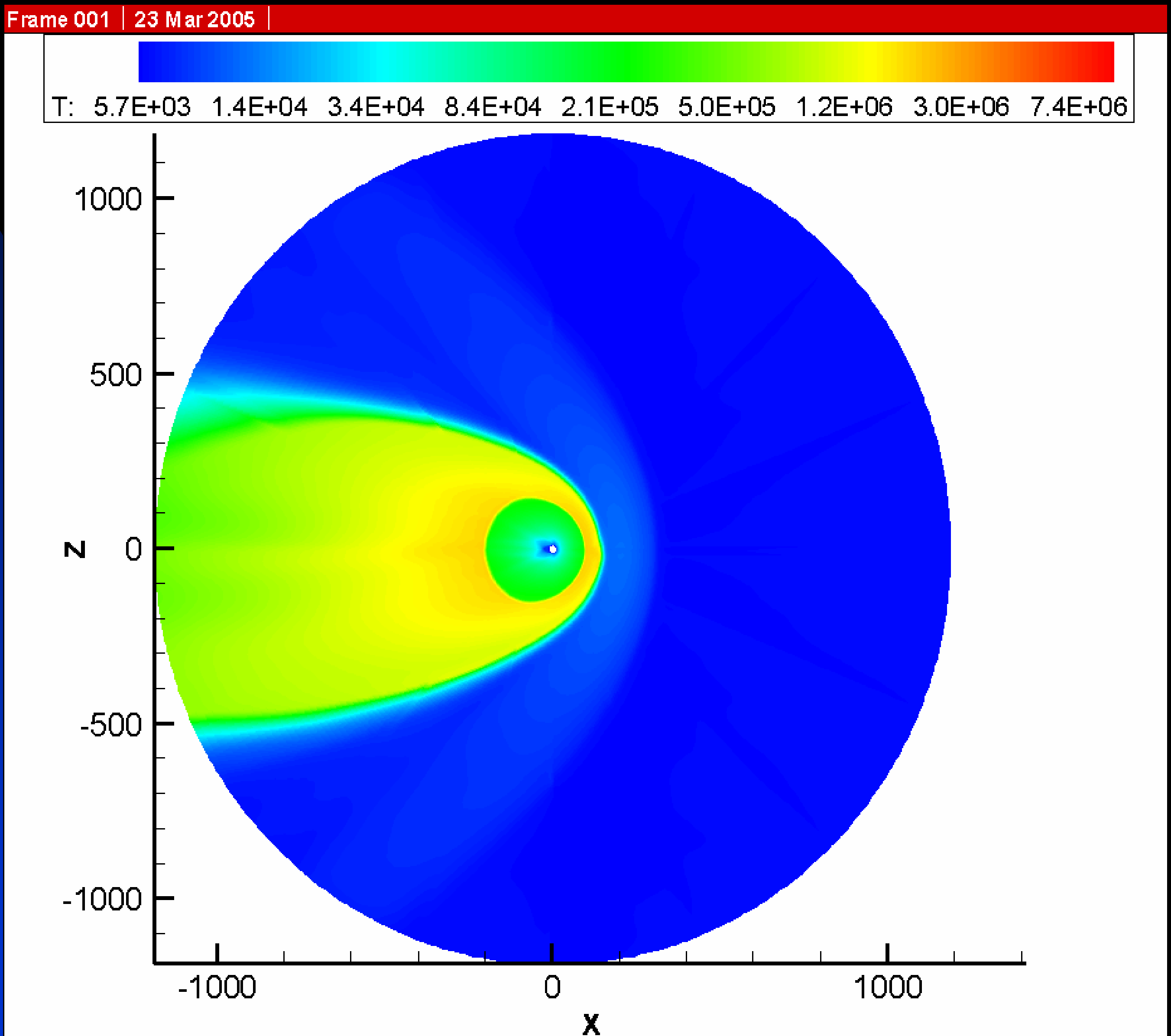

Neutral hydrogen distributions

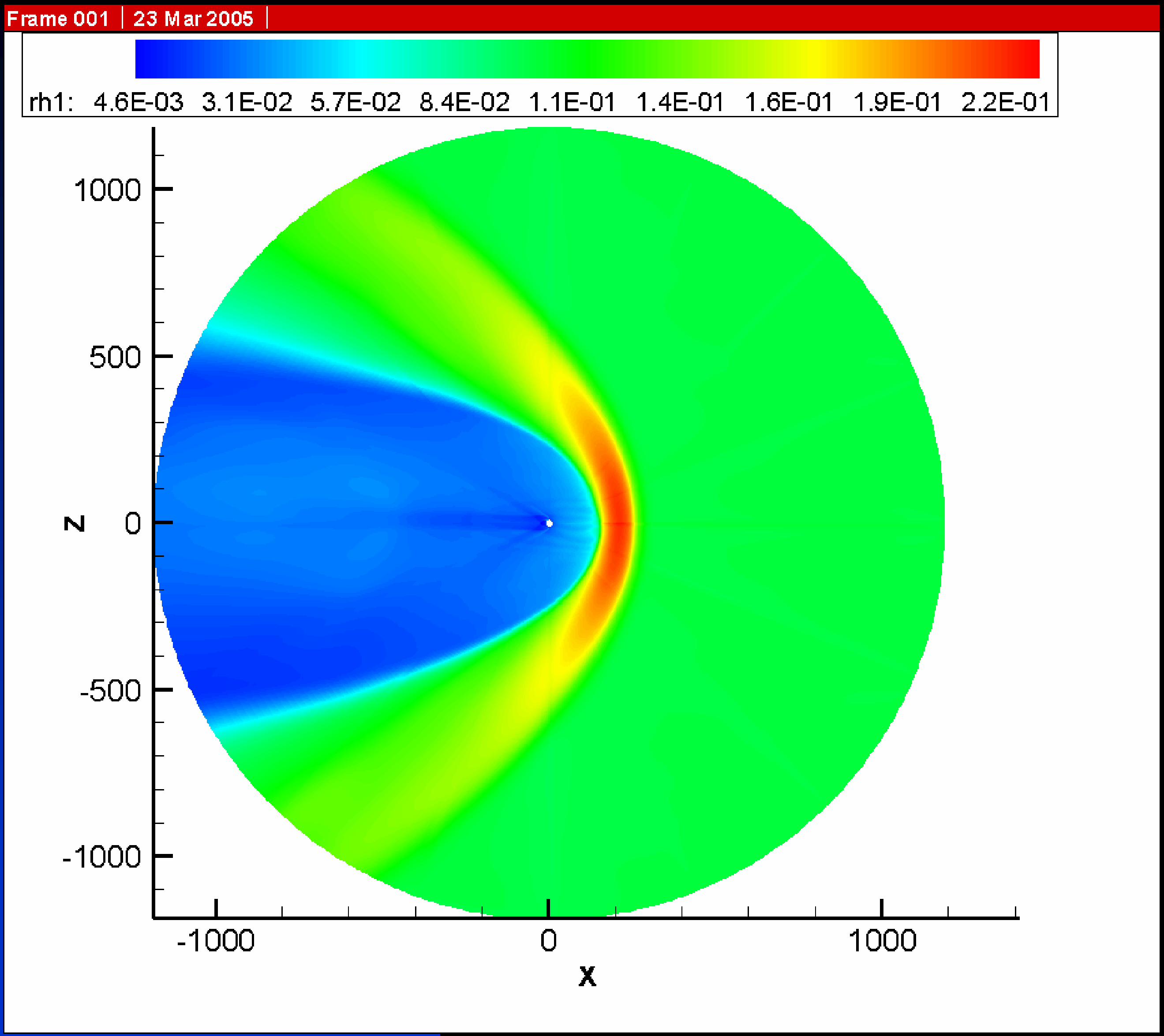

Frames 1-25:

Sequence of snapshots at t=0,

66.5,

121.7,

154.6,

179.5,

206.9,

242.7,

292.6,

346.2,

400,

and 457.5 days.

Neutral hydrogen distributions

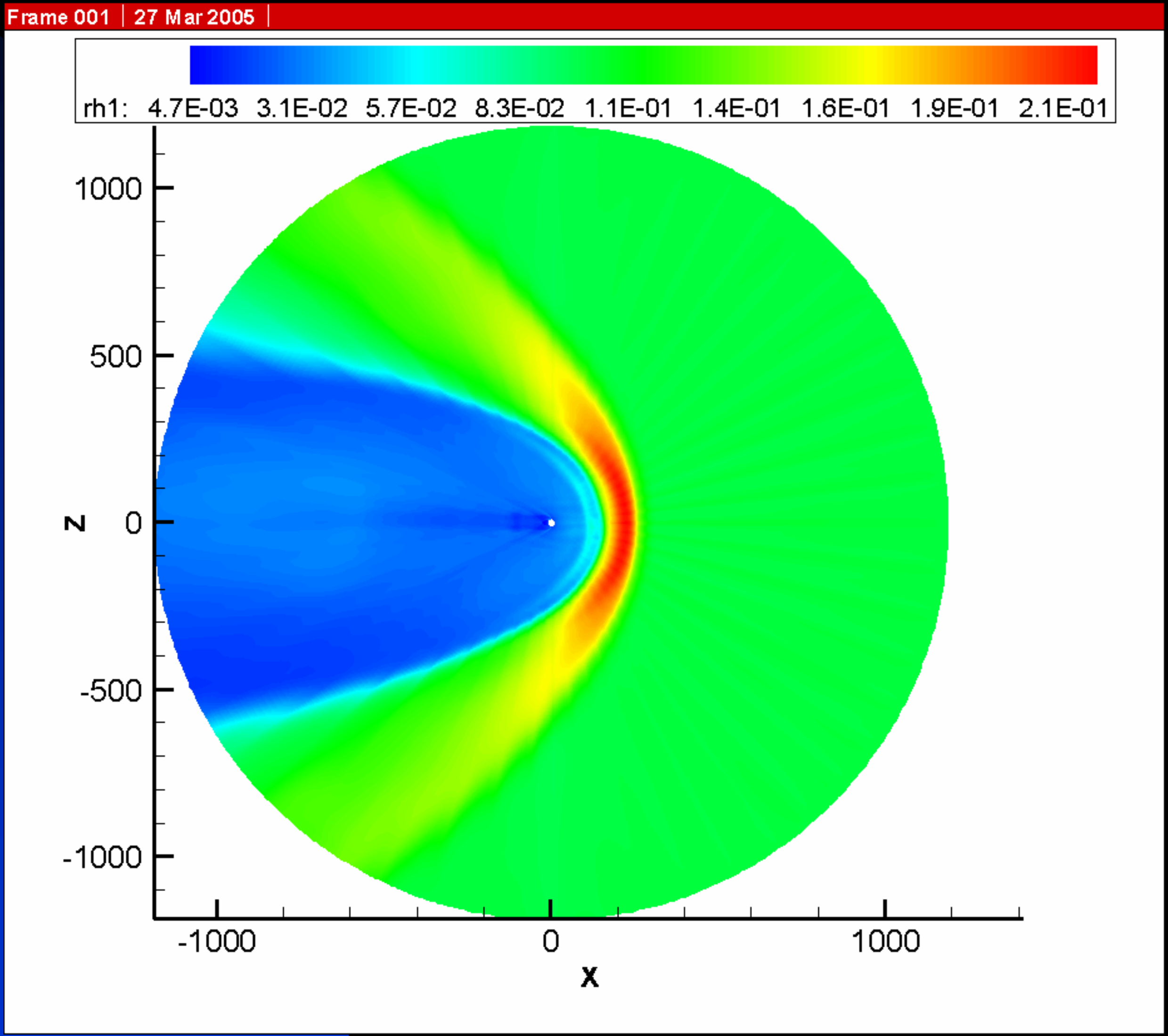

Frames 26-55

Radial distributions in different directions from the Sun

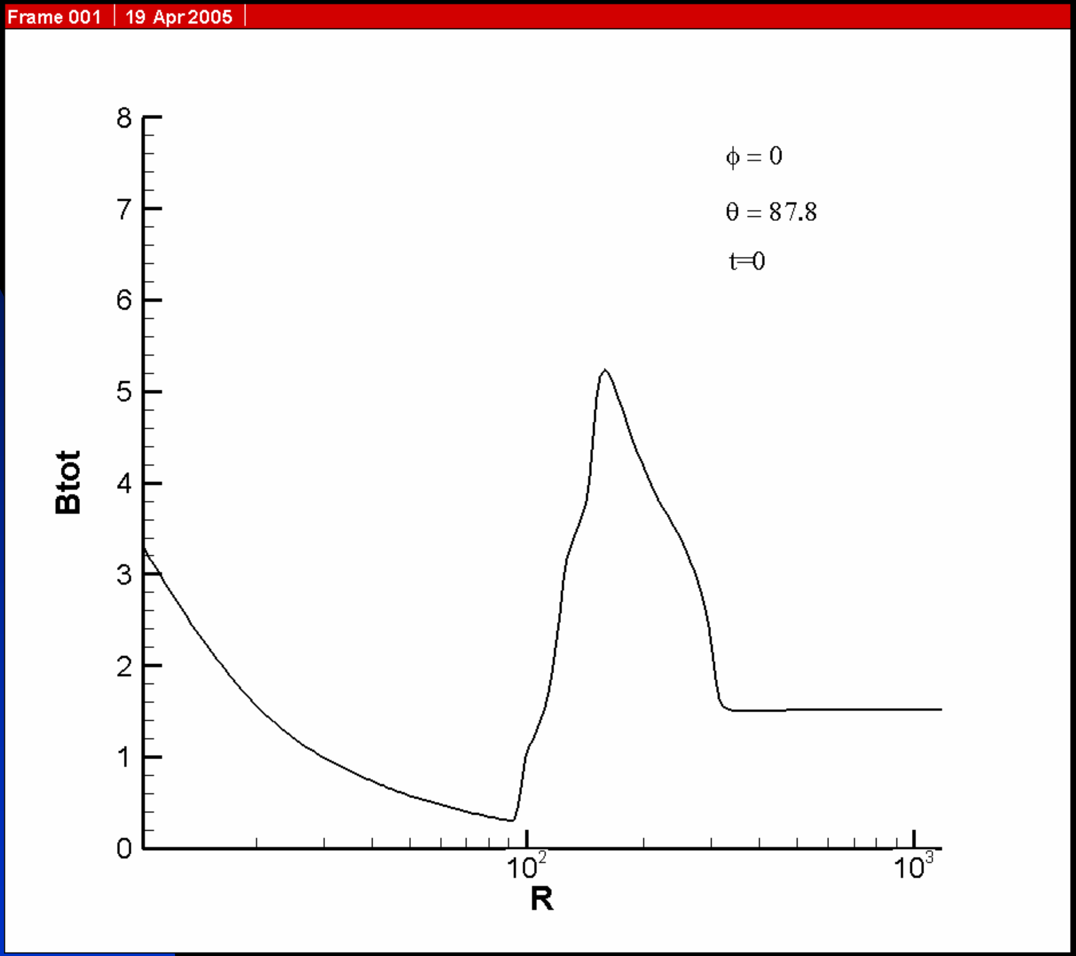

Magnetic field slightly above the ecliptic plane

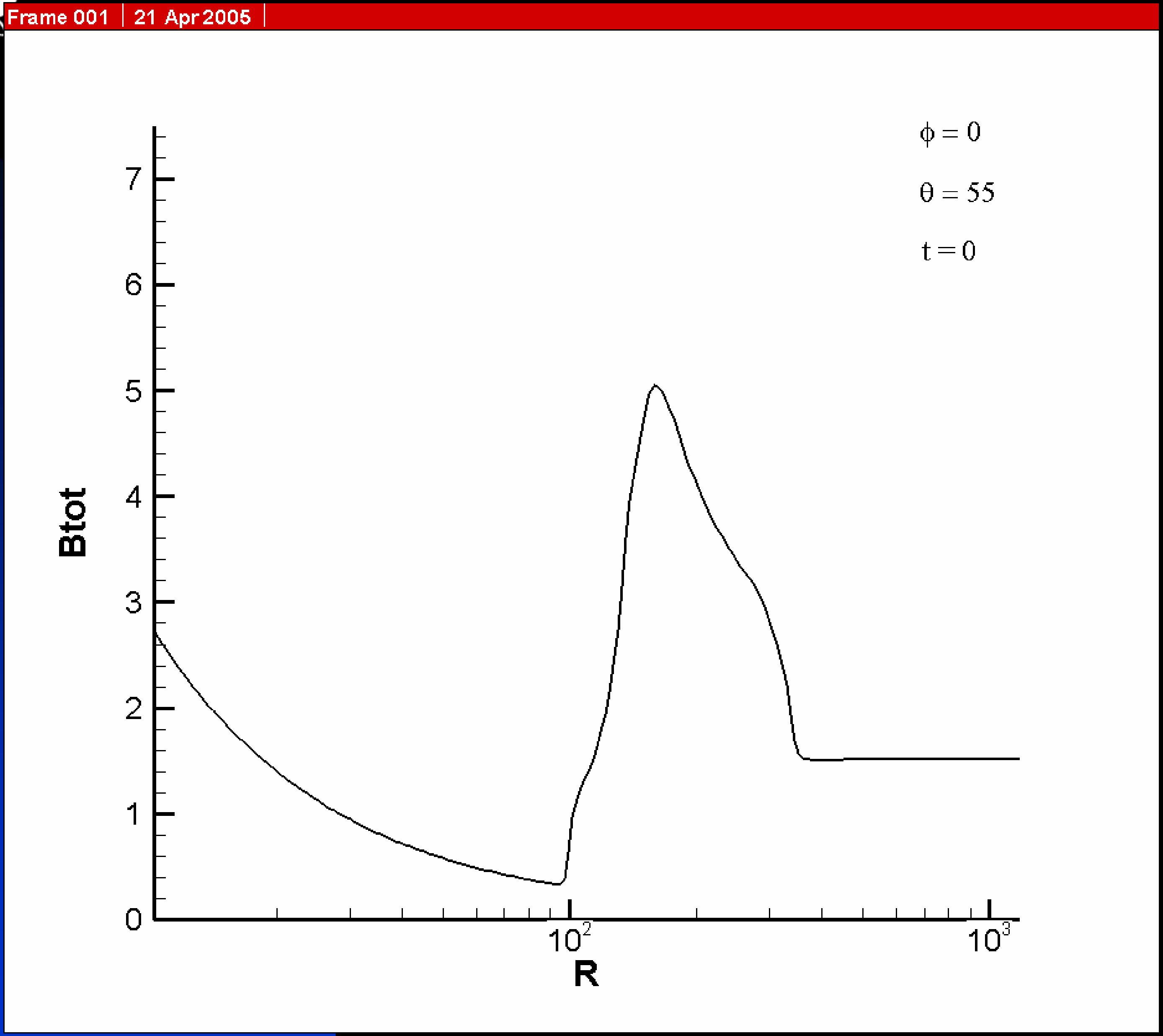

Magnetic field in the direction of Voyager 1

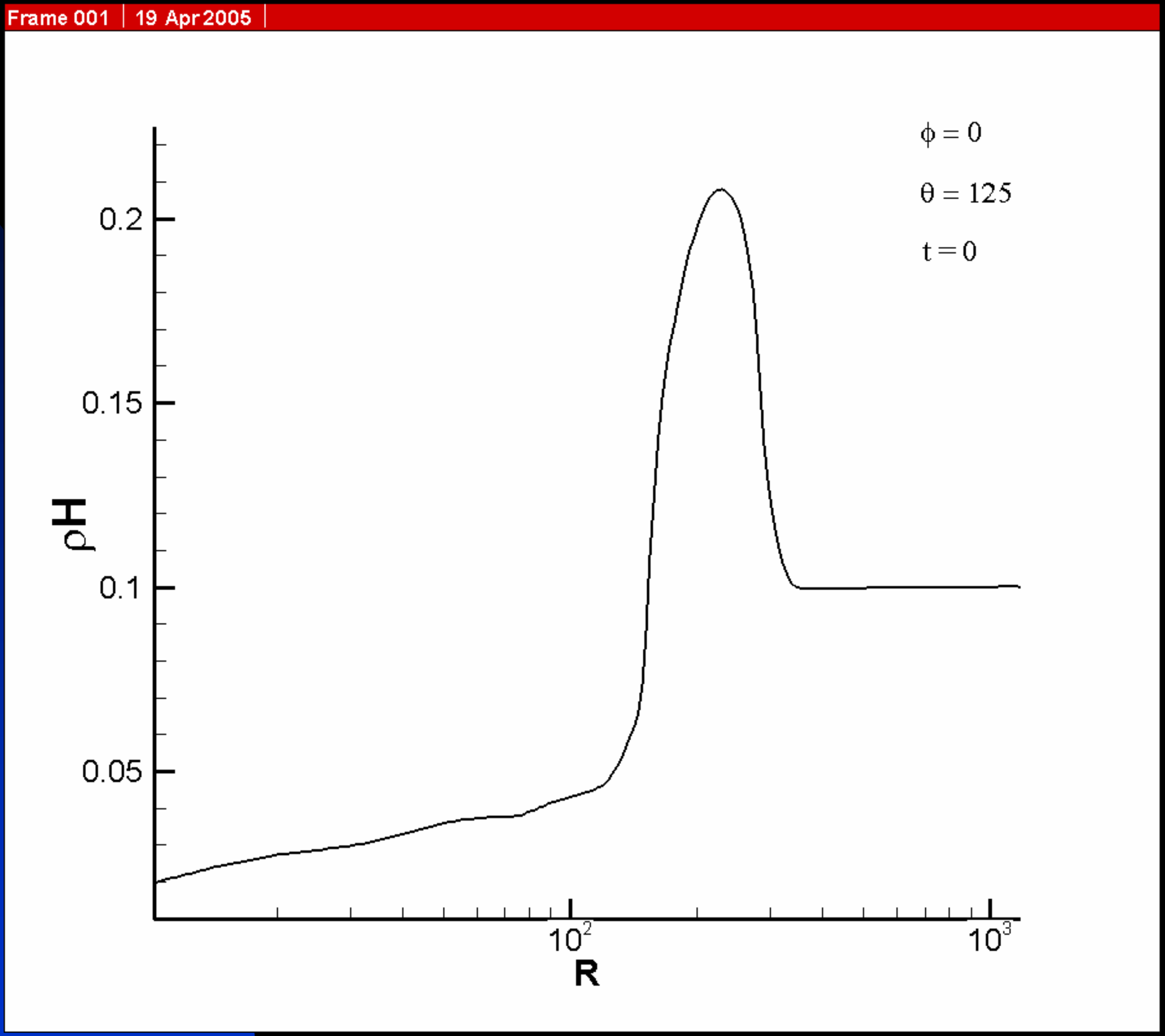

Neutral hydrogen density variation in the direction of Voyager 1

CONCLUSIONS

1. 3D calculations of GMIR propagation taking into account both interplanetary and interstellar magnetic fields. Neutral hydrogen atoms are modeled using the multi-fluid approach.

2. GMIRs create moving magnetic barriers in the solar wind region that are comparable or stronger than the compressed IMF at the inner side of the heliopause.

3. Bending of the HCS and/or IMF-ISMF lines reconnection cause substantial asymmetries in the time-dependent parameter distribution with respect to the ecliptic plane.

4. Perturbations of the heliopause lead to a noticeable increase in the ISMF strength in the outer heliosheath.

Galactic cosmic rays: global heliospheric modulation

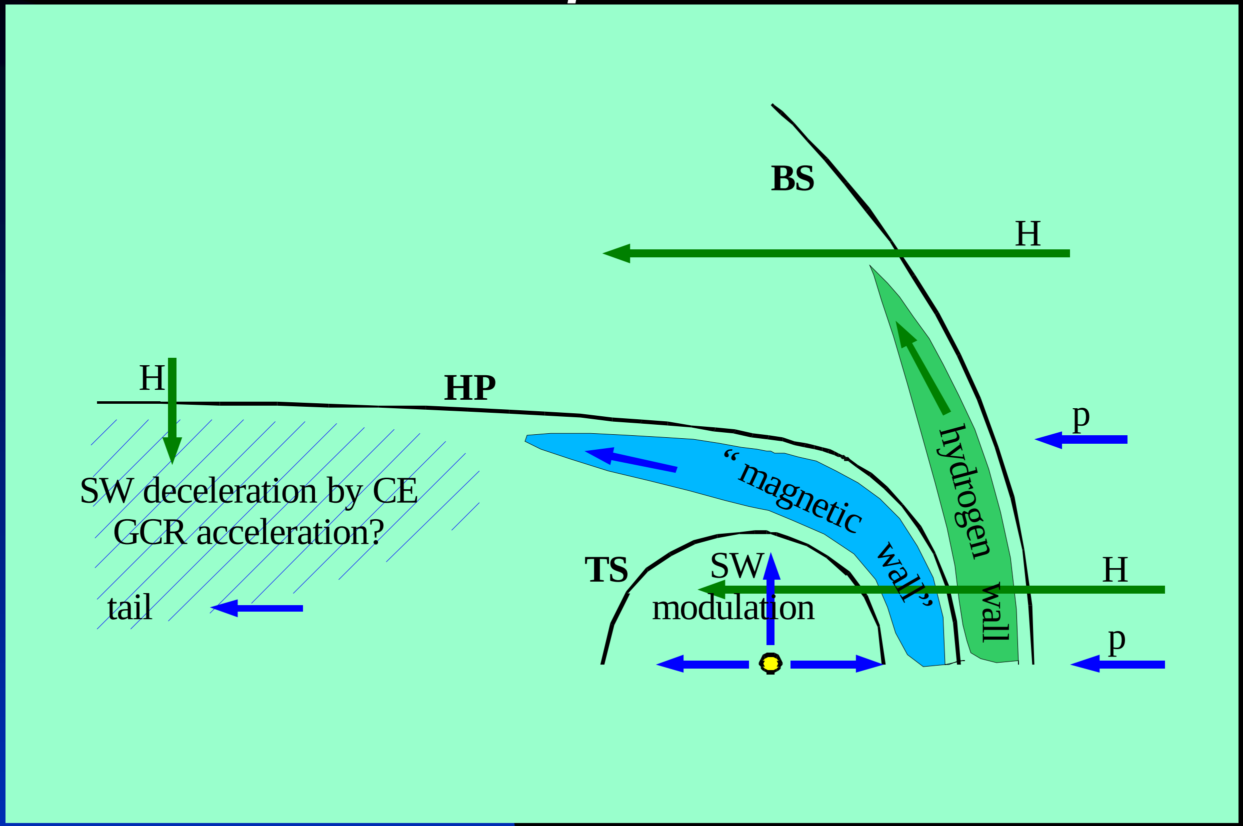

Florinski, Zank, Pogorelov, 2003

Magnetic field (B_j) is strongly amplified near the stagnation point and gets convected to higher latitudes creating a region of enhanced magnetic field (small diffusion). This is expected to filter lower energy GCR. 2D and 3D magnetic wall structures different.

Termination shock is not spherically symmetric.

Compressive flow in the heliotail caused by charge-exchange slowdown of the SW may accelerate GCR.

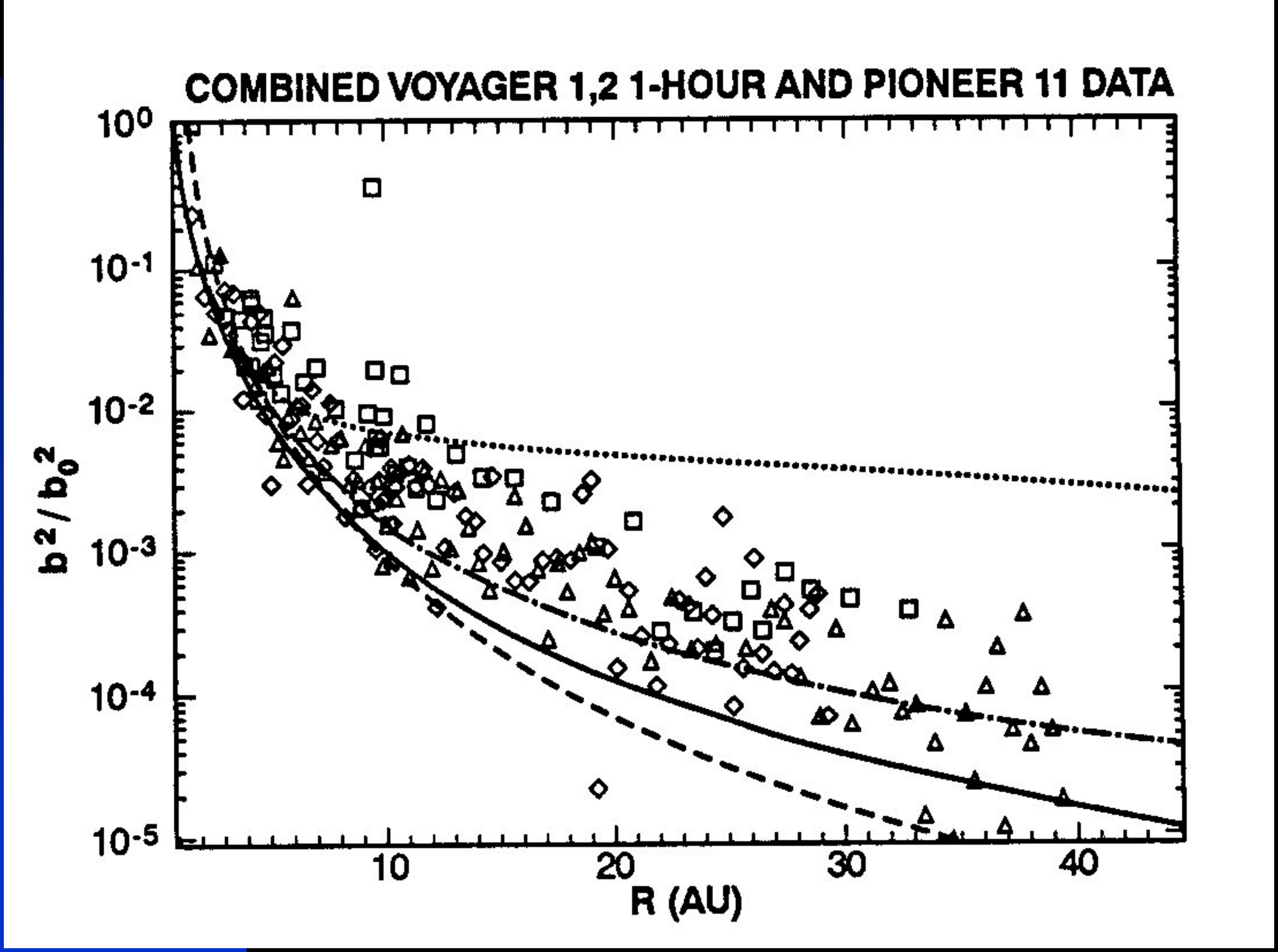
COMBINED VOYAGER 1,2 1-HOUR AND PIONEER 11 DATA
10^0
10^{-1}
10^{-2}
10^{-3}
10^{-4}
10^{-5}
b^2/b_0^2
10
20
30
40
R (AU)

Galactic cosmic rays: global heliospheric modulation

Magnetic field (interplanetary)

Note the modulation barrier

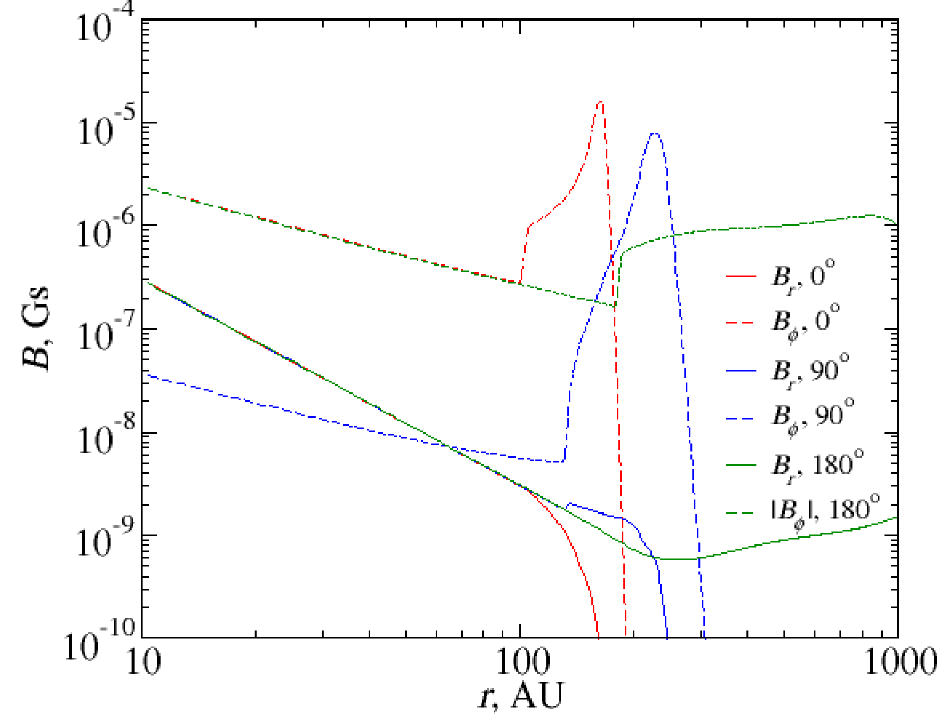

Meridional plane

Diffusion coefficients

Note that thickness of barrier (65-100 AU) is significantly larger than commonly used in modulation models.

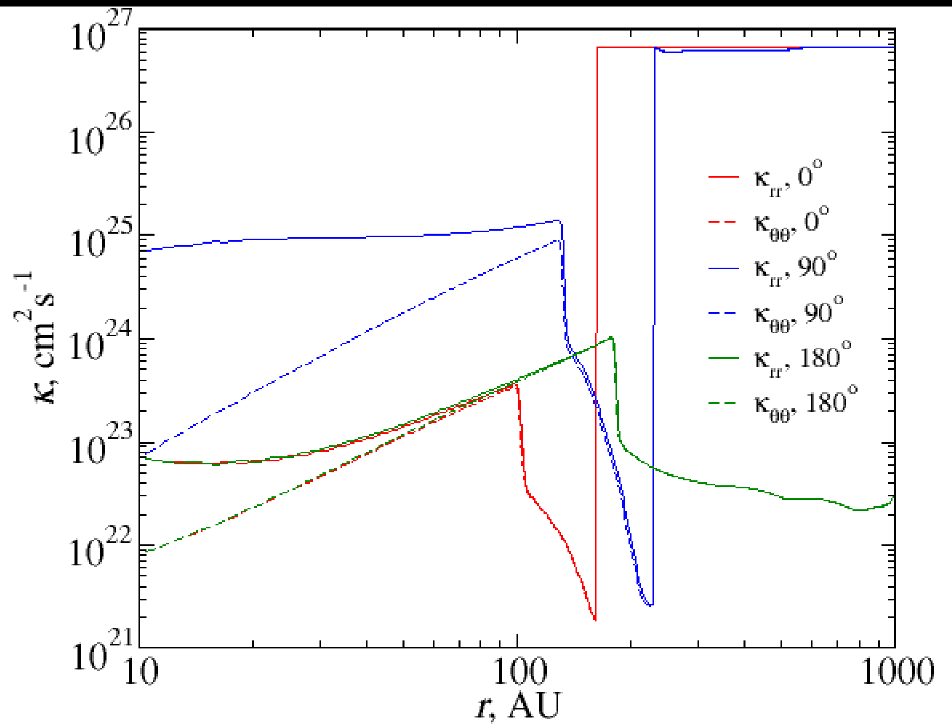

Galactic cosmic rays: global heliospheric modulation

No hydrogen atoms.

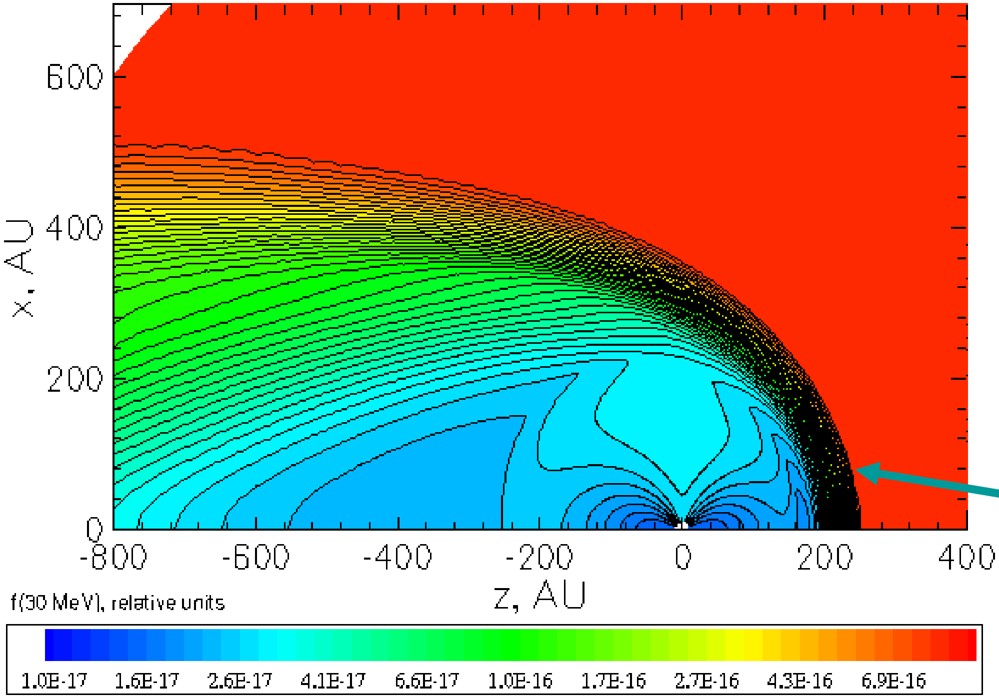

30 MeV protons

Cosmic-ray distribution in the inner heliosphere exhibits a typical "lobe" structure seen in many modulation models, which is caused by the change in kappa with heliolatitude.

Strong attenuation in the “magnetic wall” (heliosheath region).

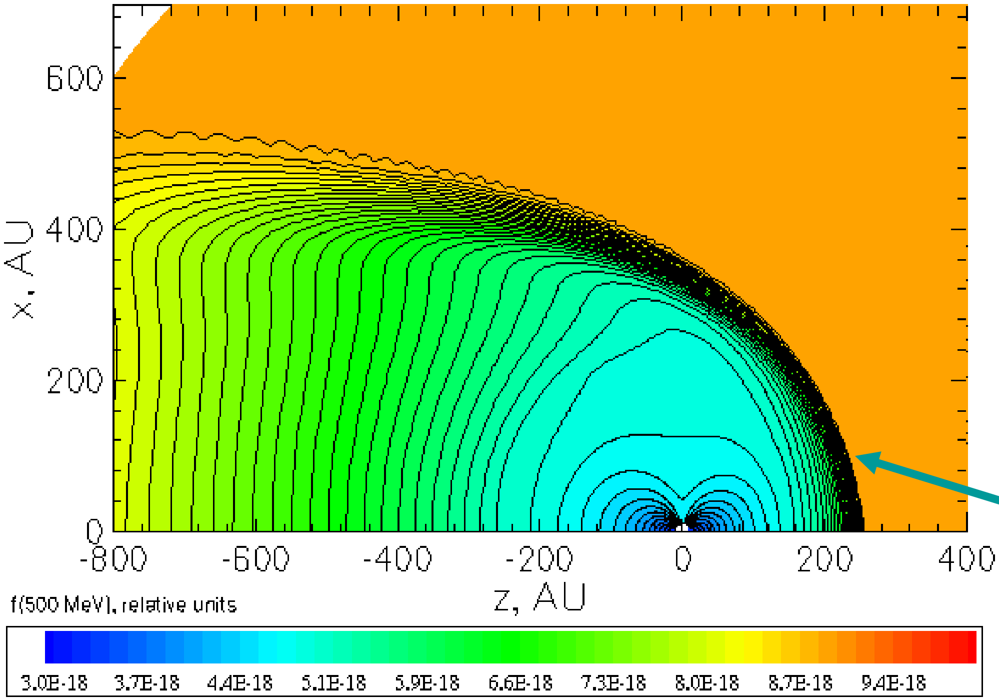

500 MeV protons

Galactic cosmic rays: global heliospheric modulation

Hydrogen atoms included.

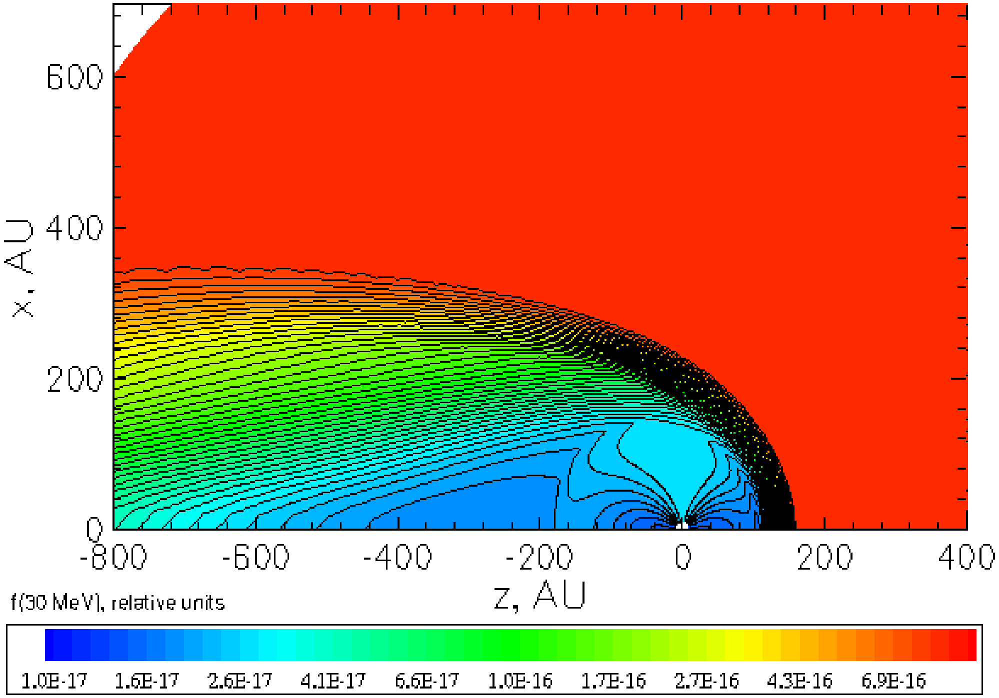

30 MeV protons

Note re-acceleration in the tail (convergent solar wind flow $\cdot \mathbf{u}<0$).

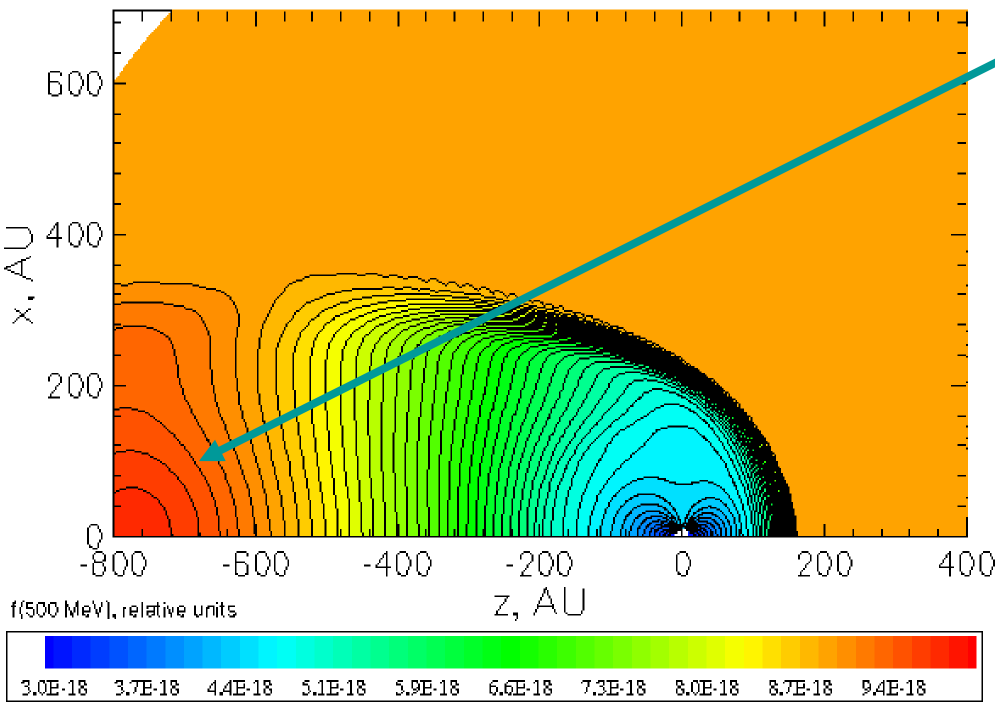

500 MeV protons

Galactic cosmic rays: global heliospheric modulation

Modulation due to heliosheath

re-acceleration

GCR spectra (H atoms included):

LISM (solid),
1.1r_s 0º (dashed),
1.1r_s 90º (dash-double-dotted),
800 AU 180º (dotted),
10 AU 0º (green).
10 AU with no H atoms (red)

Effect of the modulation cavity reduction due to neutrals is not significant (~5%) at small heliocentric distances.

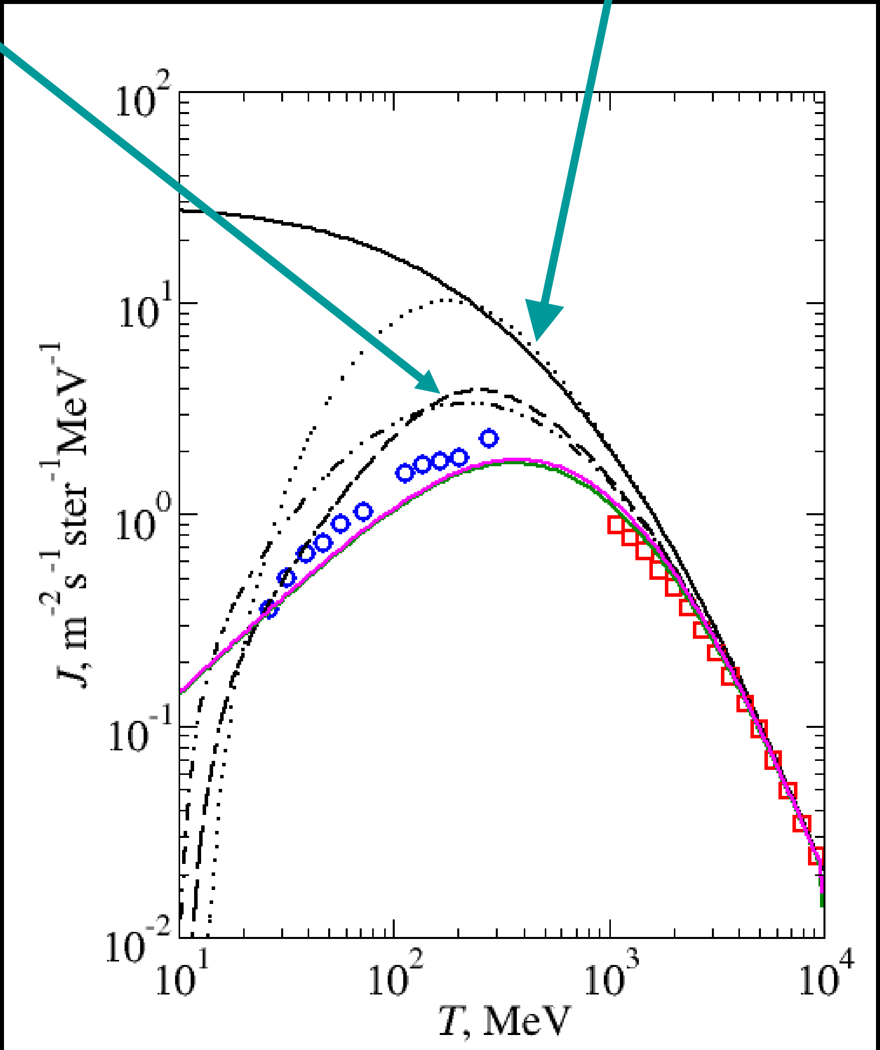

Challenges to theoretical modeling: Concluding remarks

- The physics of the neutral – plasma interaction more complicated than simple CE. Kinetic and multi-fluid approaches are converging.
- Implications of modeling heavy atoms and their coupling to ACRs
- The 3D heliosphere: solar wind anisotropy, 2D vs 3D MHD modeling, inner heliosheath structure and HP structure unresolved, structural asymmetry when LISM B field included.
- Time dependence: solar cycle, solar wind disturbances, quasi-periodicity of current sheet, unstable jet, stability of HP due to neutrals.
- Galactic cosmic rays, diffusion coefficients, and the heliospheric boundaries.